UC Berkeley
UC Berkeley Previously Published Works

Title
Measurement of Three Transport Coefficients and the Thermodynamic Factor in Block Copolymer Electrolytes with Different Morphologies

Permalink
https://escholarship.org/uc/item/58g6q7g8

Journal
The Journal of Physical Chemistry B, 124(5)

ISSN
1520-6106

Authors
Galluzzo, Michael D
Loo, Whitney S
Wang, Andrew A
et al.

Publication Date
2020-02-06

DOI
10.1021/acs.jpcb.9b11066

Peer reviewed

eScholarship.org Powered by the California Digital Library
University of California

Measurement of Three Transport Coefficients and the Thermodynamic Factor in Block Copolymer Electrolytes with Different Morphologies

Michael D. Galluzzo[1,2], Whitney S. Loo[1], Andrew A. Wang[1], Amber Walton[1], Jacqueline A. Maslyn[1,2], and Nitash P. Balsara[1,2,3]*

[1]Department of Chemical and Biomolecular Engineering University of California, Berkeley, CA 94720, United States.

[2]Materials Science Division, Lawrence Berkeley National Laboratory, Berkeley, CA 94720, United States.

[3]Joint Center for Energy Storage Research (JCESR), Lawrence Berkeley National Laboratory, Berkeley, CA 94720, United States.

AUTHOR INFORMATION

Corresponding Author

* Correspondence to: nbalsara@berkeley.edu, +1-510-642-8973

ABSTRACT

The design and engineering of composite materials is one strategy to satisfy the materials needs of systems with multiple orthogonal property requirements. In the case of rechargeable batteries with lithium metal anodes, the system requires a separator with fast lithium ion transport

and good mechanical strength. In this work, we focus on the system polystyrene-*block*-poly(ethylene oxide) (SEO) with bis(trifluoromethane)sulfonimide lithium salt (LiTFSI). Ion transport occurs in the salt-containing poly(ethylene oxide)-rich domains. Mechanical rigidity arises due to the glassy nature of polystyrene (PS). If we assume that the salt does not interact with the PS-rich domains, we can describe ion transport in the electrolyte by three transport parameters (ionic conductivity, κ, salt diffusion coefficient, D, and cation transference number, t_+^0) and a thermodynamic factor, T_f. By systematically varying the volume fraction of the conducting phase, ϕ_c between 0.29 and 1.0, and chain length, N between 80 and 8000, we elucidate the role of morphology on ion transport. We find that κ is the strongest function of morphology, varying by three full orders of magnitude, while D is a weaker function of morphology. To calculate t_+^0 and T_f, we measure the current fraction, ρ_+, and the open circuit potential, U, of concentration cells. We find that ρ_+ and U follow universal trends as a function of salt concentration, regardless of chain length, morphology, or ϕ_c, allowing us to calculate t_+^0 for any SEO/LiTFSI or PEO/LiTFSI mixture when κ and D are known. The framework developed in this paper enables predicting the performance of any block copolymer electrolyte in a rechargeable battery.

MAIN TEXT

Introduction

Polymer membranes that selectively transport small molecules are used in a variety of applications including gas separations[1,2], water purification[3,4], fuel cells[5–7], and battery electrolytes[8–13]. Beyond tuning the chemistry, branching, or size of the polymer, heterogeneous materials with novel properties can be created by adding components such as a second polymer block[14–16] or nanoparticles[17,18]. Understanding how the additional phase (or phases) impacts the

material properties is important for designing nanostructured materials with improved transport capabilities. Nanophase-separated block copolymer electrolytes have been applied to enable secondary batteries with lithium metal anodes[19]. Recharging a battery with a lithium metal anode often results in the formation of dendrites that are detrimental to battery performance and safety[20,21]. Nanostructured block copolymer electrolytes are capable of transporting ions and suppressing lithium dendrites simultaneously in lithium metal batteries[10,22]. These systems comprise mechanically rigid domains composed of a polymer such as polystyrene (PS) and soft domains capable of transporting lithium ions such as polyethylene oxide (PEO) mixed with bis(trifluoromethane)sulfonimide lithium salt (LiTFSI). Sax and Ottino developed simple expressions for quantifying the effect of nanostructure on gas diffusion using an effective medium theory[23]. These expressions serve as a starting point for quantifying ionic conductivity in block copolymer electrolytes.

It is well understood that the diffusion of molecules through nanostructured materials depends strongly on morphology[24–26]. In Fig. 1, we present schematics of the experimentally observed morphologies of a polystyrene-*block*-poly(ethylene oxide) (SEO) electrolyte as a function of composition[27–29]. We use the volume fraction of the conducting domain (*i.e.* salt dissolved in PEO), ϕ_c, to quantify composition. For $\phi_c = 0$ or $\phi_c = 1$, the system is a homopolymer of the non-conducting (PS) or conducting phase (PEO), respectively. As ϕ_c is increased from 0 to 1, we observe the following sequence of morphologies: PEO-rich spheres on a body centered cubic lattice (BCC), PEO-rich cylinders on a hexagonal lattice (HEX), double gyroid comprising a PEO-rich network in a PS-rich matrix (GYR), alternating PS- and PEO-rich lamellae (LAM), double gyroid comprising a PS-rich network in a PEO-rich matrix (GYR'), PS-rich cylinders on a hexagonal lattice (HEX'), and PS-rich spheres on a body centered cubic

lattice (BCC'). (The prime in our notation denotes that PEO/LiTFSI is the majority component.) A BCC morphology is not expected to conduct ions because the salt-containing domains are isolated. Similarly, a membrane with BCC' morphology will not be mechanically robust because the rigid PS-rich domains are not interconnected. Thus, neither BCC nor BCC' morphologies are particularly interesting for battery applications, and much research attention has been focused on morphologies where ϕ_c is close to 0.5 (i.e. GYR, LAM, and GYR'). Recent computational studies by Shen, Brown, and Hall have shown that the lamellar morphology is optimal for ion diffusion[30]. The purpose of this paper is to experimentally characterize ion transport through different morphologies.

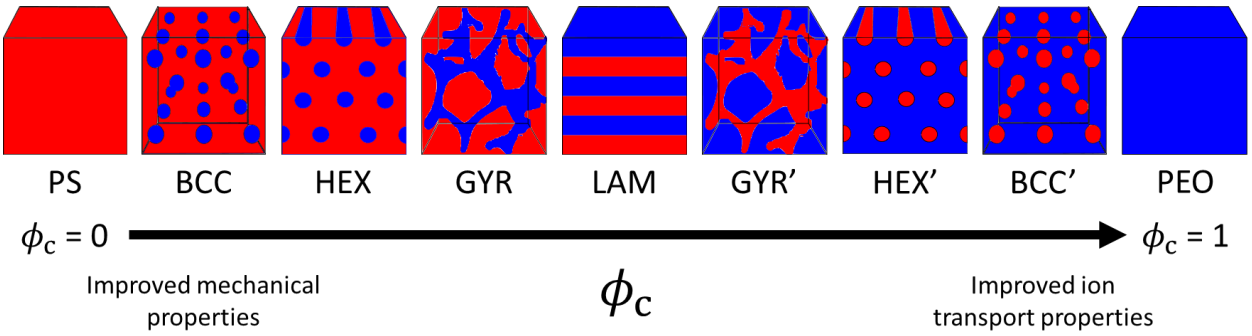

Figure 1. SEO morphologies as a function of conducting phase volume fraction, ϕ_c, with polystyrene (PS) depicted in red and poly(ethylene oxide) (PEO) with LiTFSI depicted in blue. As ϕ_c increases from ϕ_c = 0 (PS homopolymer) to ϕ_c = 1 (PEO homopolymer), the observed morphologies are: BCC – body centered cubic spheres of PEO in a PS matrix, HEX – hexagonally packed cylinders of PEO in a PS matrix, GYR – minority gyroid of PEO in a matrix of PS, LAM – alternating lamellae of PS and PEO, GYR' – minority gyroid of PS in a matrix of PEO, HEX' – hexagonally packed cylinders of PS in a matrix of PEO, BCC' – body centered cubic spheres of PS in a matrix of PEO. At low ϕ_c, the electrolytes are rigid due to the

continuous PS matrix but poor ionic conductors. At high ϕ_c, the electrolytes are highly conductive due to the continuous PEO matrix but not very rigid.

Complete electrochemical characterization of ion transport enables prediction of time-dependent salt concentration and potential gradients across a battery electrolyte during dc polarization[31,32]. A desirable electrolyte will have small salt concentration and potential gradients within the electrolyte at large current densities. Predicting the magnitude of these gradients in a homogeneous (single phase) electrolyte requires knowledge of three transport coefficients: ionic conductivity (κ), salt diffusion coefficient (D), and the cation transference number with respect to the solvent velocity (t_+^0). It also requires a thermodynamic factor defined as $T_\mathrm{f} = 1 + \frac{\mathrm{d}\ln\gamma_{+-}}{\mathrm{d}\ln m}$, where γ_{+-} is the mean molal activity coefficient of the salt and m is the salt molality in mol kg^{-1}.[31,33]. Fully characterizing transport in a nanostructured electrolyte will, in principle, require measuring many more transport and thermodynamic factors. The presence of polystyrene makes SEO/LiTFSI a four-component system (PS, PEO, Li^+, $TFSI^-$). The presence of nanophase separated domains adds additional complexity. In this paper, we make the simplifying assumption that knowledge of three transport coefficients and the T_f is adequate to describe ion transport in block copolymer electrolytes. We examine the effect of morphology and ϕ_c on each transport coefficient and T_f. We find that T_f exhibits a surprisingly complex dependence on morphology. This dependence is outside the scope of simple effective medium theories. Our approach uses concentrated solution theory[31] to develop a complete picture of ion transport based on our assumptions. The theory may be used to make testable predictions[32,34] and, in turn, validate or invalidate our assumptions. In principle, similar approaches may be applied to other problems associated with simultaneous diffusion of small molecules through nanostructured media.

Experimental Section

Polymer Synthesis and Characterization

All electrochemical and morphological characterization was carried out at 90 °C. The SEO copolymers in this study were synthesized, purified, and characterized using methods described in refs [28,35]. The polymers are referred to as SEO(*x*-*y*) for block copolymers and PEO(*y*) for PEO homopolymers, where *x* and *y* are the number-averaged molecular weights of PS, M_{PS}, and PEO, M_{PEO}, in kg mol^{-1}, respectively. The volume fractions of each block of the copolymers are calculated by:

$$\phi_{\mathrm{EO}} = \frac{v_{\mathrm{EO}}}{v_{\mathrm{EO}} + \frac{M_{\mathrm{PS}} M_{\mathrm{EO}}}{M_{\mathrm{S}} M_{\mathrm{PEO}}} v_{\mathrm{S}}} \quad , \tag{1}$$

where v_{EO} and v_{S} are the volumes of ethylene oxide (0.0682 nm^3) and styrene monomers (0.167 nm^3) and M_{EO} and M_{S} are the molar masses of ethylene oxide (44.05 g mol^{-1}) and styrene (104.1 g mol^{-1}). Monomer volumes were calculated by $v_{\mathrm{i}} = \frac{M_{\mathrm{i}}}{\rho_{\mathrm{i}} N_{\mathrm{A}}}$, where N_{A} is Avogadro's number. The densities of the PEO and PS blocks at 90 °C are ρ_{PEO} = 1.07 g cm^{-3} and ρ_{PS} = 1.03 g cm^{-3}, respectively[36]. The overall degree of polymerization, N, was calculated by $N = N_{\mathrm{PS}} + N_{\mathrm{PEO}}$ where

$$N_i = \frac{M_{\mathrm{i}}}{\rho_{\mathrm{i}} N_{\mathrm{A}} v_{\mathrm{ref}}} \tag{2}$$

and v_{ref} was fixed at 0.1 nm^3. The neat copolymers are completely transparent and colorless.

Electrolyte Preparation

The block copolymer and salt mixtures were prepared by freeze-drying using methods described in ref [37], except for SEO(240-260) and SEO(200-222) which were prepared by solvent casting[38]. All electrolyte and cell preparation was performed in an argon-filled glovebox maintained with water and oxygen concentrations below 1 ppm each. The molar ratio of lithium

ions to ethylene oxide (EO) moieties, $r = [\mathrm{Li}]/[\mathrm{EO}]$, is used in this study to quantify salt concentration. r is related to the salt molality, m, by Eqn. 3,

$$m = \frac{r}{M_{\mathrm{EO}}}. \tag{3}$$

Note that m is the molality of the PEO domains in our nanostructured electrolyte (i.e. moles of salt per kg of PEO) and it is calculated assuming that all of the salt resides in the PEO domains[39–41]. We determine the volume fraction of the salty PEO domain, ϕ_{c}, using

$$\phi_{\mathrm{c}} = \frac{\nu_{\mathrm{c}}}{\nu_{\mathrm{c}} + \left(\frac{M_{\mathrm{PS}} M_{\mathrm{EO}}}{M_{\mathrm{S}} M_{\mathrm{PEO}}}\right)\nu_{\mathrm{S}}}, \tag{4}$$

where ν_{c} is the volume of the conducting phase per EO monomer and is given by $\nu_{\mathrm{c}} = \frac{M_{\mathrm{PEO}}}{\rho_{\mathrm{c}} N_{\mathrm{A}}}$ where ρ_{c} is the density of the conducting domain at a specific salt concentration. ρ_{c} as a function of r was taken from ref [42] and we assume that the density of the conducting domain does not depend on ϕ_{c} for the SEO electrolytes. In general, ϕ_{c} increases with increasing salt concentration.

The electrolytes used in this study are listed in Table I. For each polymer we list M_{PS}, M_{PEO} and N. For each electrolyte we list r, ϕ_{c}, and the morphology at 90 °C. Information about morphology is generally based on small angle X-ray scattering (SAXS) experiments. We include the neat polymers for completeness. The morphologies of SEO(4-22.4), SEO(5.1-12.8), SEO(3.8-8.2), and SEO(9.4-4) are given in ref [29]. We have taken electrochemical and morphological data from previous studies on PEO(5) and a variety of other SEO/LiTFSI systems listed in Table I, and we list the relevant references next to the polymer name. Most of the electrolytes studied in this work exhibit the ordered morphologies presented in Fig. 1. Many of the short-chained (*i.e.* low-N) polymers are disordered (DIS) in the neat state and at low salt concentrations. The disordered morphology is characterized by fluctuating PEO-rich and PS-rich domains but with no long-range

order[43]. These fluctuations give rise to a characteristic broad scattering peak. The disordered systems listed in Table I give way to ordered morphologies with the addition of salt. All of the electrolytes are ordered when $r > 0.05$. The effect of added salt on the morphology and thermodynamics of block copolymer electrolytes is an active research topic[28,29,44–46], but is not the focus of this study. In most cases, a single morphology is present at each salt concentration. In SEO(4.0-22.4), we observe coexisting ordered morphologies as indicated in Table I.

Table I. List of electrolytes used in this study. The polymer name, molecular weight of polystyrene block (M_{PS}) in kg mol^{-1}, molecular weight of poly(ethylene oxide) block (M_{PEO}) in kg mol^{-1}, number of repeat units (N) calculated from Eqn. 2, salt concentration (r), conducting phase volume fraction (ϕ_{c}) calculated from Eqn. 4, and morphology are listed. Some electrochemical data was taken from other works, and we report the reference for those electrolytes next to the polymer name. An (') indicates that PEO is the majority phase and an (*) indicates that the morphology for that salt concentration was not determined experimentally but assumed based on ϕ_{c}.

Polymer	M_{PS}	M_{PEO}	N	r	ϕ_c	Morphology
PEO(5)[38,42]	0	5.0	77	neat	1	-
				0.005	1	-
				0.010	1	-
				0.020	1	-
				0.040	1	-
				0.060	1	-
				0.080	1	-
				0.100	1	-
				0.120	1	-
				0.140	1	-
				0.160	1	-
				0.180	1	-
				0.210	1	-
				0.240	1	-
				0.270	1	-
				0.300	1	-
SEO(4.0-22.4)	4.0	22.4	411	neat	0.84	DIS
				0.005	0.85	DIS
				0.010	0.85	DIS
				0.025	0.85	HEX'
				0.050	0.86	HEX'
				0.075	0.87	HEX'/BCC'
				0.100	0.87	HEX'/BCC'
				0.150	0.89	BCC'
				0.200	0.90	BCC'
				0.250	0.90	BCC'
				0.300	0.91	BCC'
SEO(5.1-12.8)	5.1	12.8	280	neat	0.71	DIS
				0.005	0.71	DIS
				0.010	0.71	DIS
				0.025	0.72	GYR'
				0.050	0.74	HEX'
				0.065*	0.74	HEX'
				0.075	0.75	HEX'
				0.100	0.76	HEX'
				0.150	0.78	HEX'
				0.200	0.79	HEX'
				0.250	0.81	HEX'
				0.300	0.82	HEX'
				0.350*	0.83	HEX'
SEO(3.8-8.2)	3.8	8.2	188	neat	0.67	DIS
				0.005	0.68	DIS
				0.010	0.68	DIS
				0.025	0.69	DIS
				0.050	0.70	GYR'
				0.075	0.72	HEX'
				0.100	0.73	HEX'
				0.150	0.75	HEX'
				0.200	0.77	HEX'
				0.250	0.78	HEX'
				0.300	0.80	HEX'
SEO(74-98)[47]	74	98	2707	neat	0.56	LAM
				0.085	0.61	LAM
SEO(6.0-7.0)[47]	6.0	7.0	205	neat	0.53	LAM
				0.085	0.58	LAM
SEO(200-222)	200	222	6653	neat*	0.52	LAM
				0.085*	0.57	LAM
SEO(240-260)[38]	240	260	7885	neat	0.51	LAM
				0.020*	0.52	LAM
				0.035*	0.53	LAM
				0.050*	0.54	LAM
				0.085*	0.57	LAM
				0.100*	0.57	LAM
				0.120*	0.58	LAM
				0.150*	0.60	LAM
				0.200*	0.62	LAM
				0.250*	0.64	LAM
				0.300*	0.66	LAM
SEO(16-16)[48,49]	16	16	505	neat	0.49	LAM
				0.030	0.51	LAM
				0.060	0.53	LAM
				0.080	0.54	LAM
				0.110	0.56	LAM
				0.150	0.58	LAM
				0.180	0.59	LAM
				0.210	0.61	LAM
				0.240	0.62	LAM
				0.270	0.63	LAM
				0.300	0.64	LAM
SEO(352-166)[50]	352	166	8232	neat	0.31	HEX
				0.085	0.36	HEX
SEO(247-116)[50]	247	116	5769	neat	0.31	HEX
				0.085	0.36	HEX
SEO(54-23)[50]	54	23	1225	neat	0.29	HEX
				0.085	0.34	HEX
SEO(9.4-4.0)	9.4	4.0	213	neat	0.29	DIS
				0.010	0.29	HEX
				0.025	0.30	HEX
				0.040*	0.31	HEX
				0.050	0.32	HEX
				0.065*	0.33	HEX
				0.075	0.33	HEX
				0.100	0.34	HEX
				0.150	0.37	HEX
				0.200	0.39	HEX
				0.250	0.41	HEX
				0.300	0.43	HEX
				0.350*	0.45	HEX

Electrochemical Characterization

SEO samples for electrochemical measurements were prepared by placing electrolytes in annular silicone spacers with inner diameters of 3.18 mm and hand-pressing them into pellets. Samples were hot-pressed at 90 ºC to create a uniform, non-porous films. The polymer sample was sandwiched between stainless steel or lithium electrodes of known thickness. The total cell thickness was measured using a micrometer before attaching nickel current collectors and sealing the cell in polypropylene-lined aluminum pouch material. At this point the cells were removed from the glovebox for testing. The inner diameter of the spacer and the thickness measurements allow for determination of the cell constants A and L, the electrochemically active area and distance between electrodes, respectively.

Ionic conductivity of samples with blocking electrodes (stainless steel), κ, was measured by ac impedance spectroscopy at 90 ºC using a BioLogic VMP3 potentiostat with an amplitude of 80 mV and frequency range of 1 MHz to 100 mHz. The bulk resistance, R_b, was determined by fitting an equivalent circuit and used to calculate κ from Eqn. 5,

$$\kappa = \frac{L}{R_\mathrm{b} A}\,. \tag{5}$$

Prior to measurement, cells were annealed at 120 ºC for at least 12 hours on a custom-built temperature-controlled heating stage.

Cells with lithium electrodes were used to measure the current fraction, ρ_+, as described in refs [42,51]. Our methods follow those pioneered by Bruce and Vincent[52,53]. Lithium cells were annealed for at least four hours at 90 °C followed by at least four conditioning cycles. Conditioning cycles allowed the interfacial resistance to reach a stable value that did not change with time or as current was passed. The bulk resistance (*i.e.* conductivity) remained within the reported experimental error bars throughout the conditioning cycles. Each cycle consisted of passing current

at +20 μA cm^{-2} for 4 h followed by -20 μA cm^{-2} for 4 h. ρ_+ is measured in an experiment where a constant voltage, ΔV, is applied across the cell to obtain the ratio of the current measured at steady state, i_{ss}, to the initial current given by Ohm's law, i_Ω, corrected for the change in potential drop across the electrolyte due to the change in current over the experiment. The equation used to calculate ρ_+ is given by:

$$\rho_+ = \frac{i_{\mathrm{ss}}}{i_\Omega}\frac{(\Delta V - i_\Omega R_{\mathrm{i},0}A)}{(\Delta V - i_{\mathrm{ss}}R_{\mathrm{i,ss}}A)}, \tag{6}$$

where $R_{\mathrm{i},0}$ and $R_{\mathrm{i,ss}}$ are the interfacial resistance measured by ac impedance spectroscopy before the experiment and once steady state is reached, respectively. ρ_+ is equal to the cation transference number for an ideal electrolyte at infinite dilution. Because this is never the case for practical electrolytes, we avoid calling this quantity "the transference number" as is commonly done in the literature and instead refer to it as "the current fraction"[51,54]. We measured the ionic conductivity of the cells with non-blocking (i.e. lithium) electrodes, κ_{nb}, and calculated i_Ω using Eqn. 7:

$$i_\Omega = \frac{\Delta V}{L/\kappa_{\mathrm{nb}} + R_{\mathrm{i},0}A}. \tag{7}$$

The same cells were used to measure the diffusion coefficient of the salt, D, in a restricted diffusion experiment following methods described in refs[38,42]. We measure the open circuit potential, U, over time as the salt concentration gradient relaxes and fit the data to Eqn. 8 to obtain D:

$$-\frac{\mathrm{d}\ln U}{\mathrm{d}t} = \frac{\pi^2 D}{L^2}. \tag{8}$$

Concentration cells of SEO electrolytes were prepared by placing an annular silicone spacer of 0.5 or 1.0 mm thickness onto a lithium electrode. The electrolyte was then hot pressed into the spacer at 90 °C to create a uniform film. Next, another electrode/spacer assembly was made with an electrolyte of the same SEO polymer but different salt concentration. The two assemblies were

then pressed together and aligned in such a way that the two electrolytes were in physical contact. We then measured the open circuit potential, U, of the cells at 90 °C once thermal equilibrium was achieved. The cells were made with one electrolyte fixed at a reference salt concentration of r = 0.065. The salt concentration of the second electrolyte was varied between r = 0.005 and r = 0.35 to obtain the quantity $\frac{\mathrm{d}U}{\mathrm{d}\ln m}$.

Results and Discussion

This work focuses on the electrochemical properties of nanostructured electrolyte films with thicknesses in the range of 250 to 500 μm. The relationship between conductivity and morphology in confined polymer films (<10 μm thick) has been studied in detail[55–58]. The typical length scale (domain spacing) of the ordered morphologies in block copolymers range from 10 to 100 nm. For all practical purposes, the electrolytes are isotropic comprising many randomly oriented grains. Coherent order is generally restricted to grains with a characteristic length of a few μm[59]. The morphologies depicted in Fig. 1 only show the structure within a grain.

In Fig. 2a and 2b, we present κ as a function of salt concentration for many of the polymers listed in Table I on a semi-log plot. The SEO electrolytes containing 3-dimensional (3-d) conducting pathways (BCC', HEX', GYR') are shown in Fig. 2a. The conductivity of the homopolymer, PEO(5), is shown for comparison. The inset of Fig. 2a highlights the conductivity trends at low salt concentration ($r \leq 0.05$). All three SEO copolymers presented in Fig. 2a are disordered in the neat state. The addition of salt results in the formation of ordered morphologies. The dominant morphology of each electrolyte is indicated by the schematic in the legend above the plots. For SEO(22.4-4.0), a HEX' phase emerges when salt is added. Additional salt results in the coexistence of HEX' and BCC' phases and further salt added results in a BCC' phase. For SEO(3.8-8.2) and SEO(5.1-12.8), the addition of salt results in a GYR' morphology and further

salt addition results in a HEX' morphology. These phase transitions are discussed thoroughly in ref [29]. The dependence of conductivity on salt concentration of all of the copolymers discussed in Fig. 2a is remarkably similar. At low salt concentrations, conductivity increases with increasing salt concentration due to the increase in charge carrier concentration. It is well known that the addition of salt slows down segmental relaxation of the PEO chains, and this results in a conductivity maximum in the vicinity of $r = 0.10$[60]. Qualitatively similar behavior is seen in electrolytes based on PEO homopolymer; the slight dip in conductivity in the vicinity of $r = 0.13$ in the PEO(5) data in Fig. 2a is a peculiarity of 5 kg mol^{-1} PEO homopolymer. The data obtained from different copolymers in Fig. 2a is relatively similar despite the differences in morphology discussed above. There is little difference in the conductivity of disordered and ordered block copolymer electrolytes, most apparent at $r = 0.025$ in the inset of Fig. 2a. We attribute this to the presence of large concentration fluctuations in the disordered state. It appears as if the salt molecules are localized in the PEO-rich fluctuations in the disordered state and this leads to ion transport that is not very different from that observed in weakly ordered block copolymer electrolytes. In all of the electrolytes discussed in Fig. 2a, ion transport occurs through the matrix phase of the block copolymer. It is evident that the morphology of the dispersed polystyrene domains has relatively little impact on ionic conductivity on SEO electrolytes with 3-d conducting pathways.

In Fig. 2b, we show conductivity versus salt concentration for SEO electrolytes with 2-d (LAM) and 1-d conducting pathways (HEX). We first consider the values of κ in the low r-limit. We see the same general trend in Figs 2a and 2b: κ increases with r at low salt concentrations. At high salt concentration, κ appears to approach a plateau. The conductivity of SEO(16-16) is about an order of magnitude lower than that of PEO(5) while that of SEO(9.4-4.0) is about two

orders of magnitude lower than that of PEO(5). These drops correspond to transitions from 3-d (homopolymer) to 2-d (LAM) to 1-d (HEX) conducting pathways. The conductivity of SEO(240-260) lies between SEO(16-16) and PEO(5). This effect has been previously discussed in studies of symmetric block copolymer electrolytes[11,37,47].

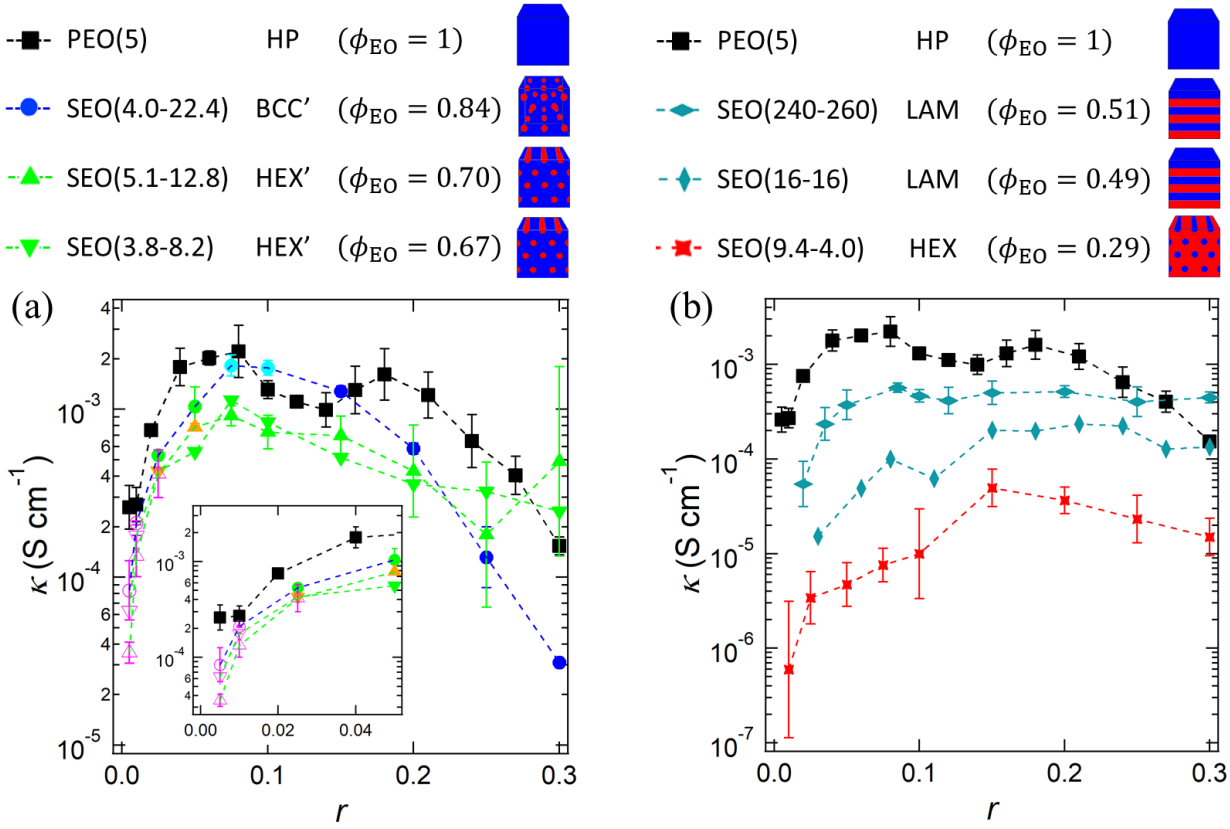

Figure 2. Conductivity, κ, of PEO and various SEO electrolytes as a function of r, the molar ratio of lithium ions to ether oxygens for the polymers listed in the figure. The color of the symbol denotes the morphology: black/homopolymer, blue/BCC', cyan/coexisting BCC' and HEX', green/HEX', gold/GYR', teal/LAM, red/HEX, purple (open)/DIS. The dominant morphology across the range of salt concentrations is indicated by the schematic in the legend above the plots. The volume fraction of the neat polymer, ϕ_{EO}, is listed in the legend and the conducting phase volume fraction, ϕ_c, of each electrolyte is given in Table 1. (a) κ vs r for PEO(5) and SEO electrolytes with 3-d conducting morphologies. The inset is a magnified view

of the low salt concentration region. (b) κ vs r for PEO(5) and SEO electrolytes with 2-d and 1-d conducting morphologies.

The conductivity of SEO/LiTFSI electrolytes is a complex function of both chain length, quantified by N, and composition, quantified by ϕ_c. In Fig. 3 we focus on the effect of chain length at two fixed compositions: ϕ_c = 0.58 ± 0.03 and ϕ_c = 0.35 ± 0.01 corresponding to LAM and HEX morphologies, respectively. The salt concentration in these electrolytes is held fixed at r = 0.085. For both morphologies, κ increases by nearly an order of magnitude when N increases from 200 to 2000. Ion transport through block copolymer electrolytes is affected by many factors including ϕ_c, the geometry of the conducting phase, the extent to which PS monomers are present in the PEO-rich conducting domains, the width of the interface between the PS-rich and PEO-rich domains[37], and the grain size[61]. The similarity of the data from LAM and HEX phases in Fig. 3 suggests a common origin for the observed increase in κ with N. The geometry of the conducting phase and ϕ_c are more or less fixed within the two data sets in Fig. 3. The presence of a large interfacial region between PS and PEO-rich domains will slow down the motion of ions that are located in the vicinity of the interface. The width of this interface decreases with increasing segregation strength (which increases with N), resulting in increased conductivity. Increasing N also results in a dramatic decrease in polymer diffusion which is necessary for eliminating defects. We thus expect smaller grains in samples with higher chain length: smaller grains also lead to an increase in conductivity in samples with 2-d or 1-d conducting pathways[50,61]. Defects are not expected to play an important role in electrolytes with 3-d conducting pathways.

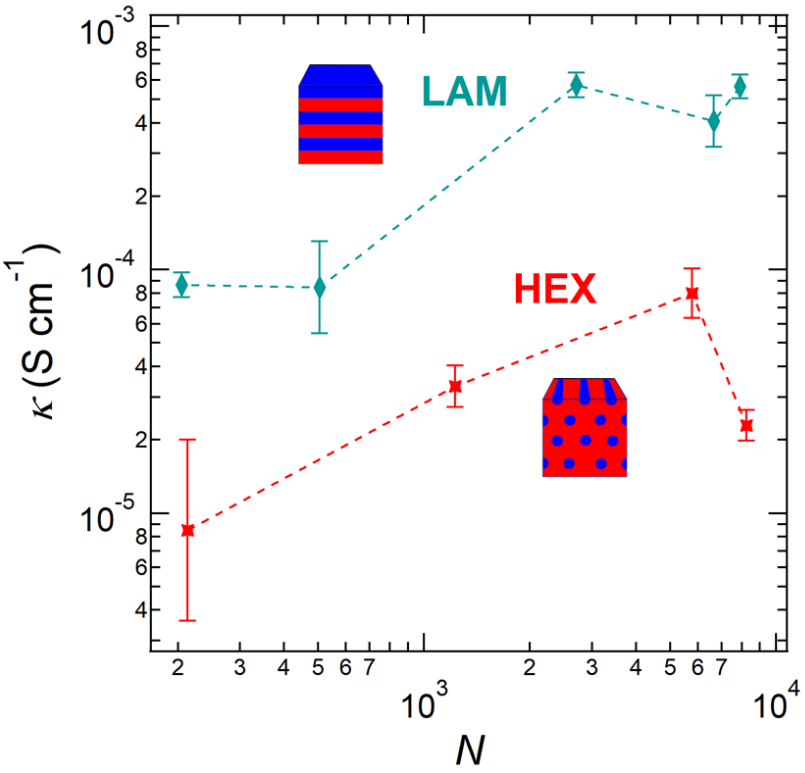

Figure 3. Conductivity, κ, of SEO electrolytes with LAM morphologies and HEX morphologies as a function of chain length, N. The salt concentration is fixed at r = 0.085 for all samples. The conducting phase volume fraction, ϕ_c, is 0.58 ± 0.03 for the LAM electrolytes and 0.35 ± 0.01 for the HEX electrolytes. For both LAM and HEX morphologies, conductivity increases by nearly an order of magnitude from N = 200 to N = 2000.

The Nernst-Einstein relationship is often invoked to relate conductivity and the self-diffusion coefficient of the ions[31]. This relationship is only applicable to ideal electrolytes in the dilute limit. (In ideal electrolytes, the salt dissociates completely to yield non-interacting ions and the salt activity coefficient of ideal electrolytes is unity.) It is well understood that polymer electrolytes do not behave ideally, even at very low salt concentrations[38,42,62]. In addition, the salt diffusion coefficient relevant to ion transport in electrolytes is a mutual diffusion coefficient, D. There may thus be little correlation between κ and D. In Fig. 4a we present D as a function of r

for the polymers with 3-d conducting domains listed in Table I, with PEO(5) included for comparison. To a good approximation, D of block copolymer electrolytes with BCC', HEX', GYR' morphologies is independent of salt concentration and not very different from that of PEO(5). In Fig. 4b, we present D as a function of r for 2-d and 1-d conducting morphologies. For the LAM morphologies, we again see that D is not a strong function of r. Similar to the trend observed for κ, we find that there is a significant increase in D for SEO(240-260) compared to SEO(16-16). There is a four-fold increase in D of SEO(9.4-4.0) when r increases from 0.06 to 0.1. We see a similar step change in conductivity in this copolymer around the salt concentration $r = 0.1$. We do not have a definitive explanation for these observations in low ϕ_c electrolytes; SAXS data across this concentration range shows no discernable change in morphology.

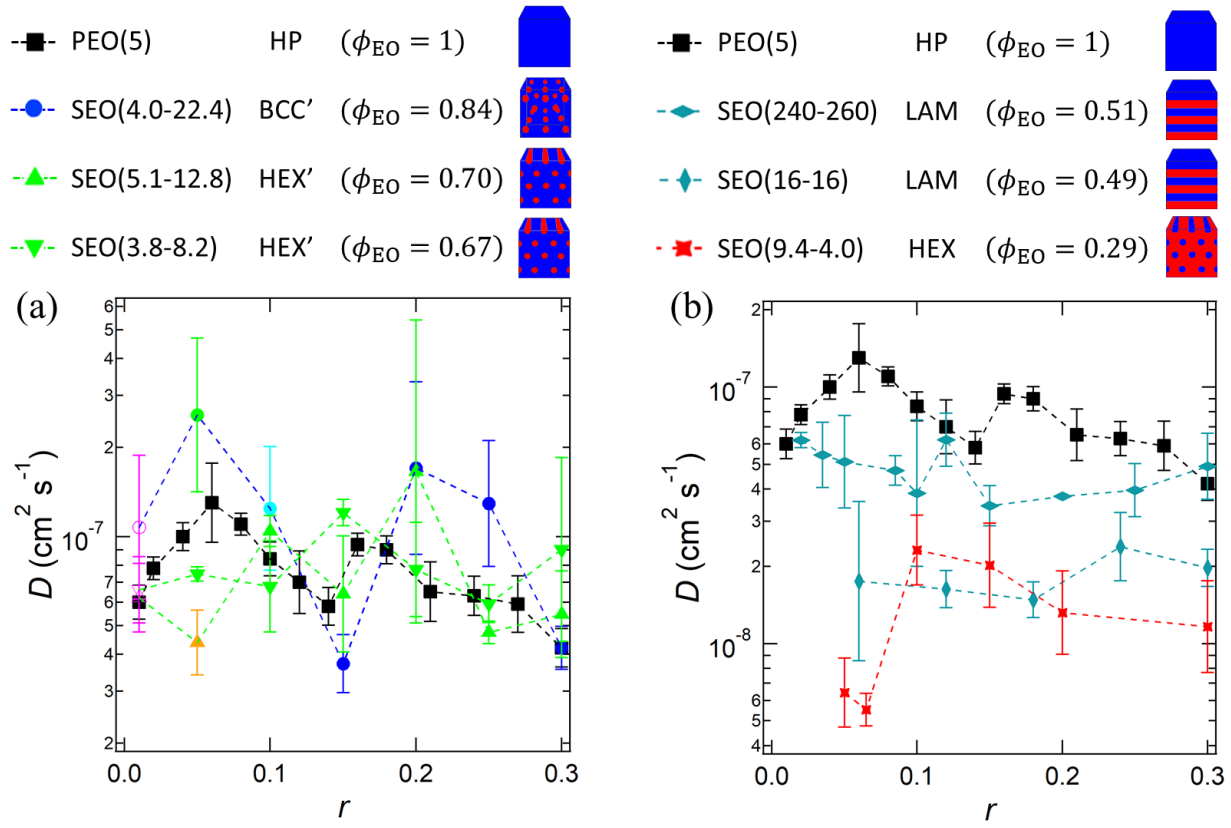

Figure 4. Salt diffusion coefficient, D, of PEO and various SEO electrolytes as a function of r, the molar ratio of lithium ions to ether oxygens for the polymers listed in the figure. The color of

the symbol denotes the morphology: black/homopolymer, blue/BCC', cyan/coexisting BCC' and HEX', green/HEX', gold/GYR', teal/LAM, red/HEX, purple (open)/DIS. The dominant morphology across the range of salt concentrations is indicated by the schematic in the legend above the plots, which is identical to the legend in Fig. 2. The volume fraction of the neat polymer, ϕ_{EO}, is listed in the legend and the conducting phase volume fraction, ϕ_c, of each electrolyte is given in Table 1. (a) D vs r for PEO(5) and SEO electrolytes with 3-d conducting morphologies. The inset is a magnified view of the low salt concentration region. (b) D vs r for PEO(5) and SEO electrolytes with 2-d and 1-d conducting morphologies.

It is useful to define κ and D for model nanostructured electrolytes and use these definitions to normalize our data[11,16,63]. We define a model nanostructured electrolyte as one where salt does not interact with the polystyrene chains and the PEO-rich nanodomains can be approximated as homopolymer electrolytes. In addition, model electrolytes comprise randomly oriented grains with negligible inter-grain resistance. We use the term "model" instead of "ideal" to avoid implying that the electrolytes are thermodynamically ideal. The thermodynamic interactions between the salt and EO monomer unit in a model nanostructured electrolyte are identical to those in PEO homopolymer, which do not behave ideally at any salt concentration. To calculate κ or D in a model morphology, we must consider how ions move within a grain and geometric factors that affect inter-grain transport of a given morphology. The baseline for our analysis is a homogeneous electrolyte sandwiched between parallel electrodes which are used to apply an electric field across the electrolyte. In a model nanostructured electrolyte, the ion moves in a tortuous path because it can only reside in a conducting domain. For 3-d conducting morphologies (i.e. GYR', HEX', BCC'), the hinderance to ion motion is quantified by a tortuosity factor, τ. The values of τ for these morphologies taken from the literature are given in

Table II. LAM and HEX phases do not have tortuous paths within a grain and $\tau = 1$. Morphology influences ion transport in these systems due to the fact that the effectiveness of each grain depends on the orientation of the grain relative to direction of the electric field. We use the morphology factor, *f*, to quantify this effect. Sax and Ottino pioneered the use of effective medium theory to calculate f in the context of diffusion of small molecules in nanostructured media[23]. Their results have frequently been applied to block copolymer electrolytes in the literature [11,30,47,48]. The values of f for LAM and HEX phases taken from ref [64] are listed in Table II. When transport occurs through the matrix phase (i.e. BCC', HEX', GYR'), we assume that f = 1. The numerical values of f and τ reported in Table II are taken from refs [30,65].

We define the conductivity, κ_{m}, and salt diffusion coefficient, D_{m}, of model nanostructured electrolytes in Eqns. 9 and 10:

$$\kappa_{\mathrm{m}}(r) = \frac{f}{\tau}\phi_{\mathrm{c}}\kappa_{\mathrm{PEO}}(r), \tag{9}$$

$$D_{\mathrm{m}}(r) = \frac{f}{\tau}D_{\mathrm{PEO}}(r), \tag{10}$$

where $\kappa_{\mathrm{PEO}}(r)$ and $D_{\mathrm{PEO}}(r)$ are transport coefficients of the PEO homopolymer at a specific salt concentration where it is assumed that the molecular weight of the PEO homopolymer is large enough so that ion transport properties are independent of molecular weight[66,67]. Physical justification for the inclusion of ϕ_{c} in Eqn. 9 but not Eqn. 10 can be found in ref [63]. Next, we define normalized transport coefficients, denoted by a subscript n, in Eqns. 11 and 12:

$$\kappa_{\mathrm{n}}(r) = \frac{\kappa}{\phi_{\mathrm{c}}\kappa_{\mathrm{PEO}(r)}}, \tag{11}$$

$$D_{\mathrm{n}}(r) = \frac{D}{D_{\mathrm{PEO}}(r)}. \tag{12}$$

Both κ_{n} and D_{n} equal $f\tau^{-1}$ for a model morphology. In Fig. 5a and 5b we present κ_{n} and D_{n}, respectively, as a function of volume fraction with r = 0.05, 0.15 and 0.30. We include the

homopolymer for completeness where $\phi_c = \kappa_n = D_n = 1$ by definition. The vertical lines separate different morphologies observed within a volume fraction range, and the solid black line represents the value of $f\tau^{-1}$.

Table II. Morphology factor, f, and tortuosity, τ, for the morphologies of interest.

Morphology	f	τ
BCC'	1	(3-ϕ_c)/2
HEX'	1	2-ϕ_c
GYR'	1	5/4
LAM	2/3	1
HEX	1/3	1

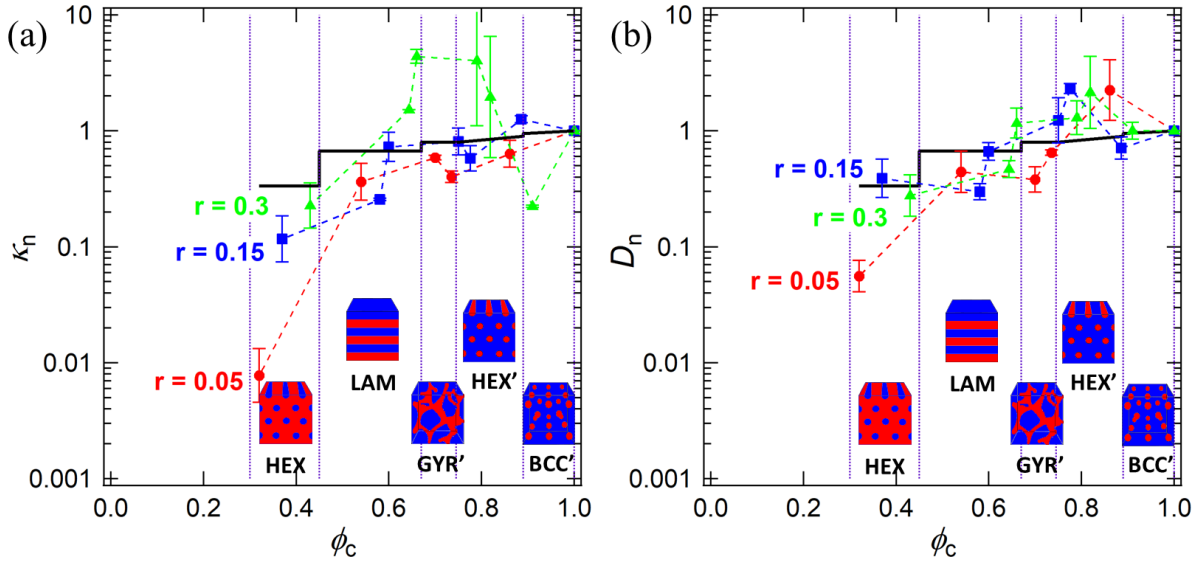

Figure 5. (a) Normalized conductivity, κ_n, and (b) normalized salt diffusion coefficient, D_n, as a function of conducting phase volume fraction, ϕ_c, for r = 0.05 (red circles), r = 0.15 (blue squares), and r = 0.30 (green triangles). The vertical lines and illustrations indicate the volume fraction range where each morphology is observed. For a model morphology, $\kappa_n = D_n = f\tau^{-1}$. We plot $f\tau^{-1}$ as a black line based on the values of f and τ given in Table II.

We discuss the data in Fig. 5a starting with the low salt concentration data set, r = 0.05. In this salt concentration regime, the normalized conductivity spans three orders of magnitude. At low ϕ_c values (i.e. the HEX morphology), κ_n is a factor of 40 below $f\tau^{-1}$. However, more reasonable agreement between κ_n and $f\tau^{-1}$ is observed once ϕ_c exceeds 0.4. Qualitatively similar behavior is seen at an intermediate salt concentration, r = 0.15; however, at low values of ϕ_c (ϕ_c < 0.45), κ_n is still a factor of 3 below $f\tau^{-1}$. At a high salt concentration, r = 0.30, we see reasonable agreement between κ_n and $f\tau^{-1}$ even at the lowest value of ϕ_c. It is evident that conductivity through block copolymers with low values of ϕ_c depends strongly on salt concentration. The measured conductivity approaches that expected for a model nanostructured electrolyte as salt concentration is increased. This observation appears to suggest that grain connectivity increases with increasing salt concentration[61]. An interesting observation is that κ_n is significantly larger than unity (i.e. κ_n = 4) for ϕ_c values of 0.67 and 0.79. This implies that the intrinsic conductivity of PEO-rich domains in the block copolymer is higher than that of PEO homopolymer electrolytes. Molecular dynamics studies have shown evidence for large ion clusters consisting of >100 ions in concentrated PEO/LiTFSI electrolytes[68]. It is not unreasonable to hypothesize that the PS domains impact the size and nature of the salt aggregates, resulting in increased conductivity. Recent coarse-grained simulations of ion transport through block copolymer electrolytes by Seo et al. suggest similar effects[69].

In Fig. 5b, we see that D_n has similar behavior to κ_n, except that the decay in D_n versus ϕ_c compared to that of κ_n is slightly less severe, especially for the HEX morphology at r = 0.05. In general, D_n tends to be close to the value of $f\tau^{-1}$ at high values of r and high values of ϕ_c. The value of D_n does not vary much with salt concentration compared to κ_n. This is because D is a much weaker function of salt concentration than κ (compare Fig. 2 and 4).

The current ratio, ρ_+, is an important electrolyte property as the product of $\kappa\rho_+$ dictates the performance of an electrolyte in the limit of small applied potentials[51–53,70,71]. In Fig. 6, we present ρ_+ for all of the polymers listed in Table I. Regardless of composition and chain length, all systems in this study show the same general trend of ρ_+ with salt concentration: ρ_+ decreases with increasing salt concentration until r is approximately 0.15 and then increases until r = 0.30. We fit a universal curve which can be used to predict the current ratio for any SEO or PEO/LiTFSI electrolyte as a function of salt concentration. The fit is shown by the black curve in Fig. 6 and is given by Eqn. 13,

$$\rho_+ = (0.18 \pm 0.01) - (1.7 \pm 0.1)r + (6.3 \pm 0.5)r^2. \quad (13)$$

Equation 13 was determined by a least-squares fit through the data in Fig. 6 and the coefficients are given with one standard deviation. Equation 13 can be used to predict the current fraction for any SEO or PEO/LiTFSI electrolyte and is valid in the salt concentration range $0.01 < r < 0.30$.

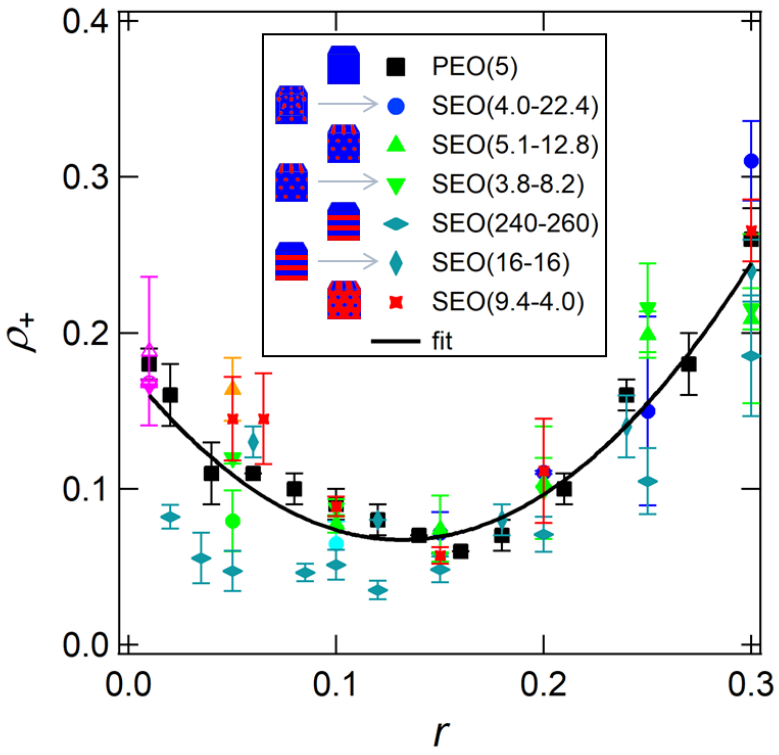

Figure 6. Current fraction, ρ_+, for PEO(5) and various SEO electrolytes as a function of r, the molar ratio of lithium ions to ether oxygens. The color of the symbol denotes the morphology: black/homopolymer, blue/BCC', cyan/coexisting BCC' and HEX', green/HEX', gold/GYR', teal/LAM, red/HEX, purple (open)/DIS. The dominant morphology across the range of salt concentrations is indicated by the schematic in the legend. Presence of the non-conducting phase does not have a significant impact on the value of ρ_+ and we are able to fit a universal curve through the data (black line). The solid curve is given by $\rho_+ = 0.18 - 1.7r + 6.3r^2$.

The current fraction is often equated to the cation transference number with respect to the solvent velocity, t_+^0. Much work, however, suggests that there is little correspondence between ρ_+ and t_+^0, especially in polymer electrolytes which exhibit behavior of non-ideal solutions even at low salt concentrations[38,42,62,72]. To calculate t_+^0, we use Eqn. 14,

$$t_+^0 = 1 + \left(\frac{1}{\rho_+} - 1\right)\frac{(z_+\nu_+)FDc\phi_c}{\kappa_{nb}}\left(\frac{dU}{d\ln m}\right)^{-1}, \tag{14}$$

where z_+ is the charge on the cation and ν_+ is the number of cations in the dissociated salt, F is Faraday's constant (96,485 C mol^{-1}), and c is the molar salt concentration in the conducting domain[31,38,73]. The quantity $c\phi_c$ is equivalent to the moles of salt per unit of total volume (*i.e.* both the conducting and non-conducting domain). c is calculated by Eqn. 15,

$$c = \frac{\rho_{PEO} r}{M_{EO} + r M_{LiTFSI}}, \tag{15}$$

where M_{LiTFSI} is the molar mass of LiTFSI (287.08 g mol^{-1}).

Ion transport in a block copolymer electrolyte is governed by numerous transport coefficients as discussed in the Introduction. Equation 14 is strictly applicable to model nanostructured electrolytes. The limitations of this approach are evident in Fig. 5 where deviations from model behavior are seen especially in the low ϕ_c and low r limit.

Calculating t_+^0 from Eqn. 14 requires measurement of κ, D, ρ_+, and $\left(\frac{dU}{d\ln m}\right)^{-1}$. In principle, κ is an intrinsic property of the electrolyte and does not depend on the electrodes used to measure it by ac impedance spectroscopy. In practice, we find some differences in the conductivity measured with blocking electrodes, κ, compared to that measured with non-blocking electrodes, κ_{nb}, at some salt concentrations. We compare these values in Fig. 7 for (a) SEO(4.0-22.4), (b) SEO(5.1-12.8), (c) SEO(3.8-8.2), and (d) SEO(9.4-4.0). The general trends discussed above in the context of Fig. 2 apply to the data in Fig. 7. The largest difference between κ and κ_{nb} is seen in SEO(9.4-4.0) at r = 0.10. However even for this electrolyte, κ and κ_{nb} are within experimental error for $r \geq 0.15$. Differences between κ and κ_{nb} may arise for block copolymer electrolytes due to differences in the morphology of the block copolymer at the electrode-electrolyte interface or differences in thermal history (see Experimental section). We note in passing that discrepancies between κ and κ_{nb} are found in many instances throughout the literature but without discussion[51,74–76]. For consistency, we use κ_{nb} for the conductivity in Eqn. 14 for calculating t_+^0 in SEO(4.0-22.4), SEO(5.1-12.8), SEO(3.8-8.2), and SEO(9.4-4.0) because measurement of D, ρ_+, and $\left(\frac{dU}{d\ln m}\right)^{-1}$ must be done in a cell with lithium electrodes.

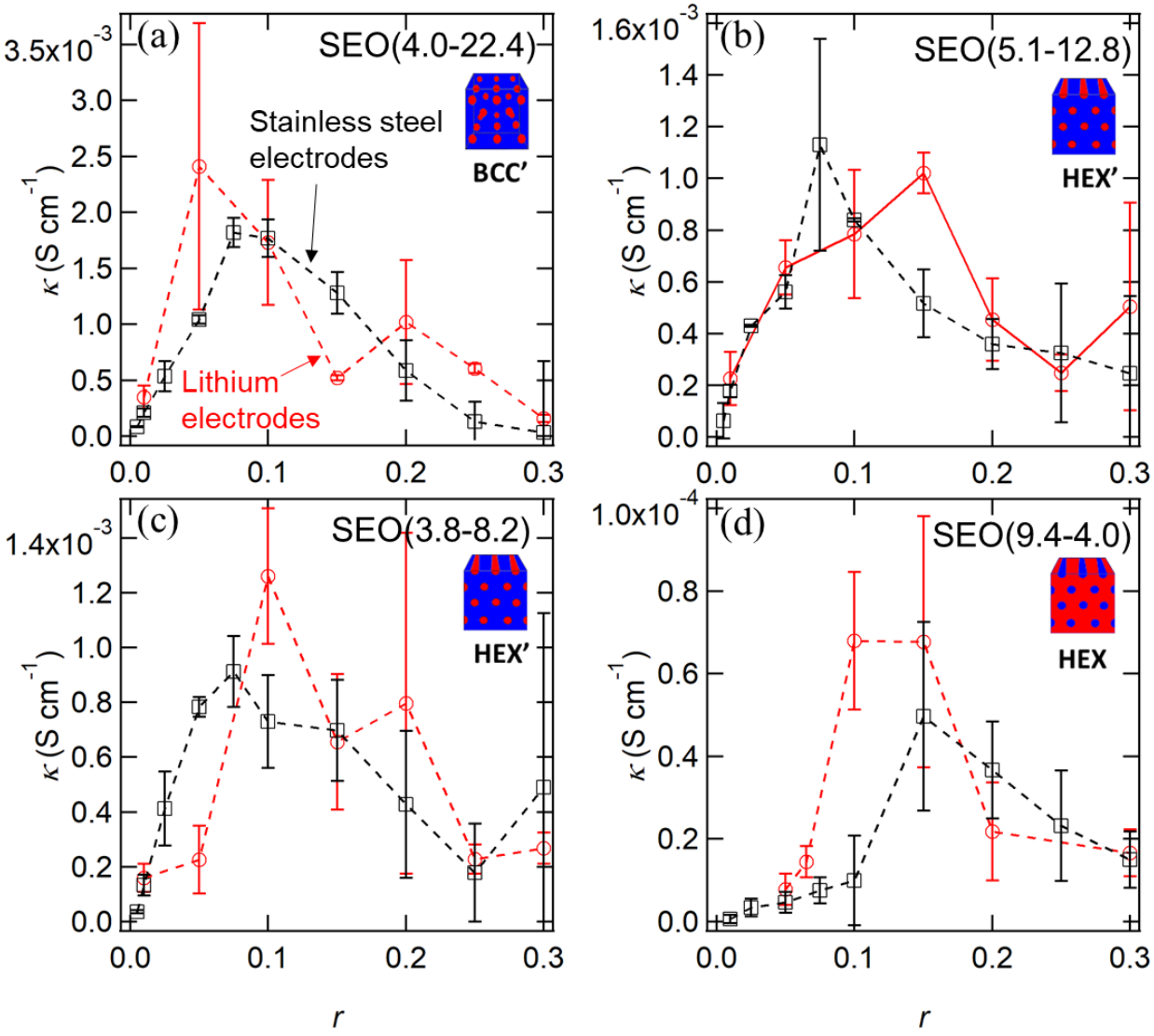

Figure 7. Conductivity, κ, measured by ac impedance spectroscopy for (a) SEO(4.0-22.4) which exhibits a BCC' morphology over most salt concentrations, (b) SEO(5.1-12.8) which exhibits a HEX' morphology over most salt concentrations, (c) SEO(3.8-8.2) which exhibits a HEX' morphology over most salt concentrations, and (d) SEO(9.4-4.0) which exhibits a HEX morphology over most salt concentrations. We compare data obtained using lithium/polymer/lithium cells (non-blocking electrodes, red circles) and stainless steel/polymer/stainless steel cells (blocking electrodes, black squares) for each system.

In Fig. 8, we present U as a function of the logarithm of the salt molality, $\ln m$, measured in concentration cells for SEO(9.4-4) and SEO(5.1-12.8) using a reference electrolyte salt molality, m_{r}, of 1.47 mol kg^{-1} (r = 0.065). The slope of U at a given value of $\ln m$ is independent of the reference salt concentration. Choosing a different reference salt concentration results in a vertical shift of U[77]. Therefore, we can include data from previous studies by plotting $U(\ln m)$ with a vertical offset, U', such that $U'(\ln m) = U(\ln m) + C$. We solve for the constant, C, by setting $U'(\ln m)$ = 0 at m = 1.47 mol kg^{-1} where $U(\ln m)$ is given by a polynomial fit through the data. For SEO(16-16), $U(\ln m)$ was reported in ref [49] with m_{r} = 0.681 (r = 0.030) and we obtained C = 43.0 mV. For SEO(240-260), $U(\ln m)$ was reported in ref [38] with m_{r} = 1.93 (r= 0.085), and we obtained C = -17.5 mV. For PEO(5), $U(\ln m)$ was reported in ref [42] with m_{r} = 1.36 (r = 0.060), and we obtained C = 14.6 mV.

We find that U is remarkably consistent across all five systems with ϕ_{c} varying from 0.3 to 1 and N varying from 80 to 8000. This suggests that the presence of polystyrene does not affect the potential of the concentration cell, and a universal relationship can be used to determine $\frac{\mathrm{d}U}{\mathrm{d}\ln m}$ for any SEO or PEO/LiTFSI mixture, regardless of morphology, ϕ_{c}, or N. We fit a single curve through the data in Fig. 8 to obtain the function:

$$U = (25 \pm 5) - (74 \pm 7)(\ln m) - (33 \pm 2)(\ln m)^2 - (4.6 \pm 2)(\ln m)^3. \qquad (16)$$

Equation 16 was determined by a least-squares fit through the data in Fig. 8 and the coefficients are given with one standard deviation. The coefficients are given with one standard deviation. Equation 16 is used to calculate $\frac{\mathrm{d}U}{\mathrm{d}\ln m}$, which is the last piece of information needed to calculate t_+^0 according to Eqn. 14. Uncertainty in using Eqn. 16 to calculate $\frac{\mathrm{d}U}{\mathrm{d}\ln m}$ is greater near the

bounds of the data set, especially at the lower bound, so we limit use of Eqn. 16 to the range -0.80 < $\ln m$ < 1.9 (*i.e.* 0.02 ≤ r ≤ 0.3).

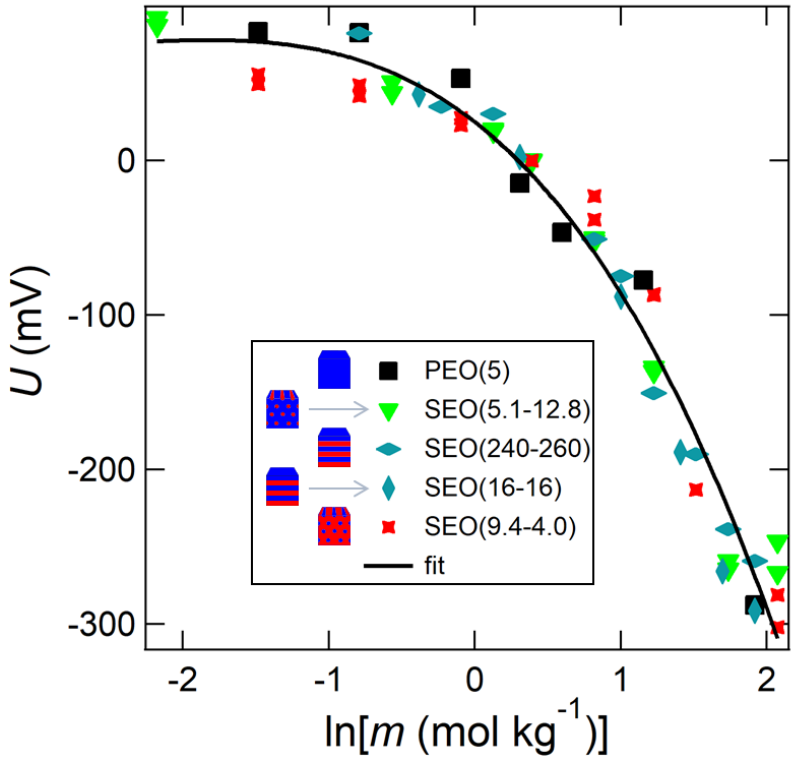

Figure 8. Open circuit potential, U, of concentration cells plotted against the natural log of the salt molality, $\ln m$, where m is in mol kg^{-1}. Each data set is vertically offset by a constant such that U = 0 at $\ln m$ = 0.39 (*i.e.* r = 0.065). We fit a universal curve through the data (black line), given by Eqn. 16: $U = 25 - 74(\ln m) - 33(\ln m)^2 - 4.6(\ln m)^3$.

We next consider the effect of morphology and ϕ_c on t_+^0 at salt concentrations ranging from r = 0.05 to r = 0.30 in Fig. 9a. We calculate t_+^0 from Eqn. 14 for SEO(4-22.4), SEO(5.1-12.8), SEO(3.8-8.2) and SEO(9.4-4) electrolytes using κ_{nb} reported in Fig. 7, D reported in Fig. 3, ρ_+ given by Eqn. 13, c given by Eqn. 15, and $\frac{d\,U}{d\ln m}$ given by taking the derivative of Eqn. 16. t_+^0 has been reported elsewhere for PEO(5), SEO(16-16), and SEO(240-260) electrolytes; however, we recalculate it using the universal relationships presented in this work for ρ_+ and U.

We use κ presented in Fig. 2 for these systems because measurements of κ_{nb} were not available. We plot t_+^0 as a function of ϕ_c in Fig. 9a at various salt concentrations. At low values of ϕ_c, t_+^0 is negative. Increasing ϕ_c results in a maximum around $\phi_c = 0.6$ for all salt concentrations. At low salt concentrations (*e.g.* $r = 0.05$), t_+^0 is a weakly decreasing function of ϕ_c above $\phi_c = 0.6$, and the maximum is relatively shallow. At intermediate salt concentrations (*e.g.* $r = 0.20$), t_+^0 decreases rapidly above $\phi_c = 0.6$, reaching a minimum in the vicinity of $\phi_c = 0.8$. At high salt concentrations (*e.g.* $r = 0.30$), the behavior is similar to that seen at low salt concentrations. If the SEO electrolytes behaved as model nanostructured electrolytes, then t_+^0 would be independent of ϕ_c and equal to that of homopolymer electrolytes, represented in Fig. 9a by the values at $\phi_c = 1$. The horizontal dashed lines in Fig. 9a show the behavior expected for model electrolytes at each salt concentration.

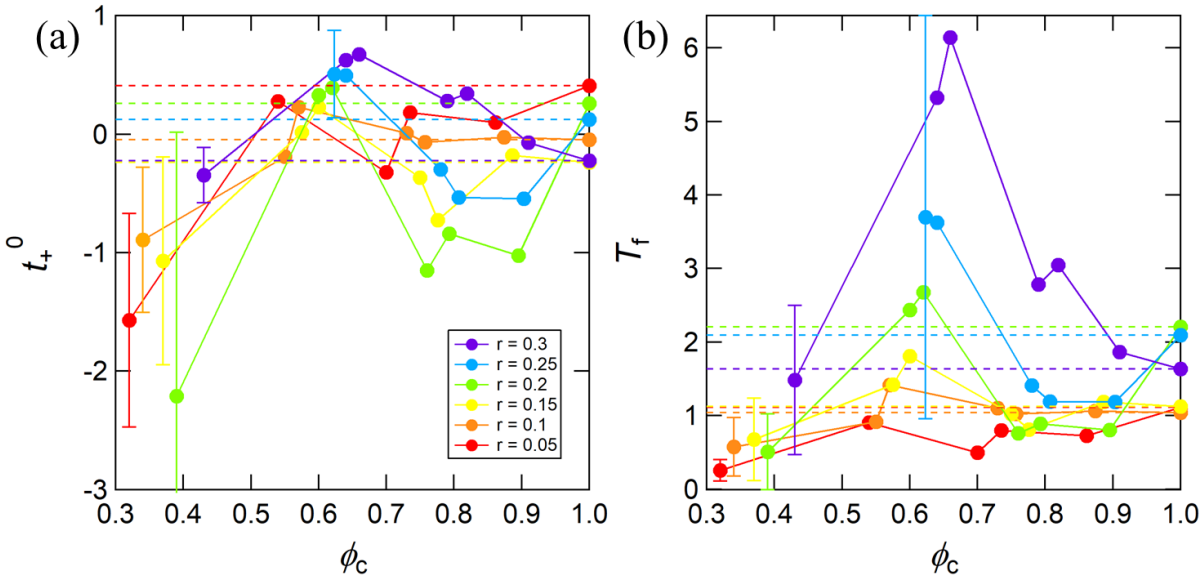

Figure 9. (a) Cation transference number, t_+^0, and (b) thermodynamic factor, T_f, of various SEO morphologies as a function of conducting phase volume fraction, ϕ_c, at salt concentrations ranging from $r = 0.05$ to $r = 0.30$. t_+^0 and T_f are calculated based on Eqn. 14 and 17, respectively.

Error bars on the first data point of each data series represent the average percent error for the entire data set. The horizontal dashed lines represent the value of t_+^0 and T_f predicted for model nanostructured electrolytes.

A negative transference number implies the presence of negatively charged ion clusters (containing both Li^+ and $TFSI^-$ ions) which are more mobile than free cations. Molinari et al. showed that large ion clusters with a net negative charge appeared more frequently in PEO/LiTFSI electrolytes than ion clusters with a net positive charge[68], providing computational evidence for this hypothesis. t_+^0 is negative and significantly lower than other morphologies for the hexagonally packed PEO cylinders (SEO(9.4-4)) across all salt concentrations (see the range $0.32 < \phi_c < 0.43$ in Fig. 9a), indicating that negatively charged ion clusters especially dominate in this system. Electrolytes with values of t_+^0 in the vicinity of unity are expected to operate with minimal salt concentration gradients.

We calculate the thermodynamic factor, $T_f = 1 + \frac{d \ln \gamma_{+-}}{d \ln m}$, for these systems from Eqn. 17:

$$T_f = -\frac{z_+ \nu_+}{(\nu_+ + \nu_-)} \frac{F}{2RT(1-t_+^0)} \left(\frac{d\, U}{d \ln m}\right), \tag{17}$$

where R is the ideal gas constant and ν_- is the number of anions in the dissociated salt. As with Eqn. 14, Eqn. 17 only applies to model nanostructured electrolytes. We plot T_f as a function of ϕ_c in Fig. 9b. Here we see a clear trend with increasing salt concentration. At low salt concentrations, T_f is a weak function of ϕ_c. At high salt concentrations, T_f exhibits a pronounced maximum in the lamellar region (ϕ_c between 0.55 and 0.65). The amplitude of the maximum increases systematically with increasing salt concentration. For a thermodynamically ideal electrolyte (nanostructured or homopolymer), $T_f = 1$. It is clear that the SEO electrolytes are far from thermodynamic ideality, especially at high salt concentrations. In theory, T_f of model

nanostructured electrolytes should be independent of ϕ_c and equal to that of the homopolymer PEO electrolyte at the same salt concentration. The dashed horizontal lines represent the theoretical value for model nanostructured electrolytes. These horizontal lines emanate from the data points at ϕ_c = 1 in Fig. 9b.

The error bars on the first data point in each series in Fig. 9 represent the average percent error for that particular data set. The uncertainty is propagated from the measurements of κ, ρ_+, D, and U, where the error for ρ_+ and U is obtained from the standard deviations of the fit coefficients from the fits in Figs. 6 and 8. Note that we have used a single function to describe the dependence of ρ_+ and U on salt concentration irrespective of the electrolyte. While the percent errors of t_+^0 and T_f are relatively large, the general trends that we have noted above are consistent across all of the salt concentrations and block copolymer compositions covered in this work.

The thermodynamic factor plays an important role in ion transport as it relates the salt concentration gradient, ∇c, to the electrochemical potential gradient of the electrolyte, $\nabla \mu_e$. This can be seen by combining Eqns. 12.12 and 12.13 of ref [31] to obtain the expression:

$$c\nabla\mu_e = \left[(\nu_+ + \nu_-)RT\left(1 - \frac{d\ln c_0}{d\ln c}\right)\nabla c\right]T_f, \tag{18}$$

where $\mu_e = \nu_+\mu_+ + \nu_-\mu_-$ is the electrochemical potential of the electrolyte, μ_+ and μ_- are the electrochemical potentials of the cation and anion, respectively, and c_0 is the solvent concentration. The product of the salt concentration and the gradient of the electrochemical potential of the electrolyte, $c\nabla\mu_e$, is the driving force per unit volume for transport of the salt. It is evident from Eqn. 18 that, for a fixed concentration gradient (∇c), an electrolyte with a large value of T_f will have a relatively strong driving force to relieve the concentration gradient.

We conclude this section by reviewing the literature on ion transport in nanostructured block copolymer electrolytes. Irwin et al. examined the relationship between morphology and κ by blending different amounts of PS and PEO homopolymer with a symmetric SEO block copolymer doped with LiTFSI to obtain LAM, HEX, bicontinuous microemulsion, and disordered phases[24]. Their results suggest that reducing long range order and thus resistance across grain boundaries results in increased conductivity, which is consistent with the trend of normalized conductivity with salt concentration in Fig. 5a. Morris, Gartner, and Epps have used tapered block copolymer electrolytes to demonstrate the relationship between conductivity and the glass transition temperature[78]. Park and coworkers have demonstrated that introducing strongly interacting end groups to block copolymers can be used as a tool to tune morphology while holding N and ϕ_c constant[79]. The resulting LAM and GYR morphologies show similar conductivities, in agreement with Fig. 5a and previous work[80]. Interestingly, end-group functionalization has a substantial impact on ρ_+[81]. In an early study, Cho and coworkers used amphiphilic dendrons containing linear PEO doped with lithium triflate salt which exhibit thermally accessible phase transitions to probe the structure-conductivity relationship[25]. Conductivity increases by a factor of six across the 1-d HEX to 3-d GYR transition in this system, which is a two times larger increase than predicted by effective medium theory. Osuji and coworkers have demonstrated that a magnetic field can be used to align the conducting domains of a PEO-based liquid crystalline diblock copolymer electrolyte, and they compared the conductivity of aligned systems relative to systems with randomly oriented grains. They find a ten-fold increase in conductivity for the HEX morphology[26] and two-fold increase for the LAM morphology[82], suggesting that deviations from model nanostructured electrolyte behavior are far more prominent in the HEX morphology with randomly oriented grains. These results are

consistent with our observation of unexpectedly low conductivity for the HEX morphology in SEO (see Fig. 5a).

Conclusions

The nature of small molecule transport through polymer membranes is complicated when the membrane consists of two (or more) distinct phases. For the simplest case where the small molecule is insoluble in the second phase, we can perhaps make the simplification that the inert phase only serves to divert the paths of the small molecules. For a block copolymer electrolyte doped with a lithium salt, this simplification allows us to assume a three component system (solvent, cation, and anion) wherein ion transport is governed by the ionic conductivity, κ, salt diffusion coefficient, D, cation transference number with respect to the solvent velocity, t_+^0, and thermodynamic factor, T_f and the role of the insulating phase is quantified by the tortuosity, τ, and morphology factor, f. Such a system is termed a model nanostructured electrolyte. We use this framework to fully characterize ion transport in a library of SEO/LiTFSI electrolytes (summarized in Table I) with different conducting phase volume fractions, ϕ_c, and chain lengths, N. By systematically varying ϕ_c and N to obtain electrolytes with different morphologies and measuring the transport properties, we can begin to elucidate the role of the insulating (PS) phase.

Our results show that κ and D are strong functions of morphology while the current fraction, ρ_+, and $\frac{\mathrm{d}U}{\mathrm{d}\ln m}$ from concentration cells do not depend on morphology. The quantities ρ_+ and $\frac{\mathrm{d}U}{\mathrm{d}\ln m}$ are required to calculate t_+^0 and T_f. We fit universal curves through data from PEO/LiTFSI and multiple SEO/LiTFSI systems for these parameters. These fits should apply to any SEO/LiTFSI or PEO/LiTFSI mixture. Measurements of κ and D from SEO block copolymer electrolytes with different morphologies can be presented on the same plot using a normalization scheme presented in Eqns. 11 and 12. We compare experimental measurements of the

normalized quantities κ_{n} and D_{n} to predictions based on values of τ and f for model nanostructured electrolytes in Table II (see Fig. 5). Experimental data for t_+^0 and T_{f} based on the assumption of model electrolytes are given in Fig. 9. Deviations from model behavior are most evident at low salt concentrations in κ_{n} (see Fig 5a). Conversely, the largest deviations from model behavior are seen at high salt concentration for T_{f} (see Fig 9b). This suggests that, at low salt concentration, the structure of the block copolymer (including morphology, grain boundaries, defects, etc.) results in ion transport through the conducting domain that is fundamentally different than that which occurs in PEO homopolymer with the same salt concentration. Conversely, at high salt concentrations, the presence of the PS domains result in thermodynamic interactions of the salt which are fundamentally different than that which occurs in PEO homopolymer at the same salt concentration.

The framework developed in this paper enables predicting the performance of any block copolymer electrolyte in a rechargeable battery. Further work[32,34] is required to test these predictions.

LIST OF SYMBOLS

A	electrochemical active area of a cell (cm^2)
BCC	body centered cubic morphology with PEO-rich spheres
BCC'	body centered cubic morphology with PS-rich spheres
c	salt concentration in the conducting phase (mol cm^{-3})
c_0	solvent concentration in the conducting phase (mol cm^{-3})
C	constant offset applied to U versus $\ln m$ data (mV)
D	salt diffusion coefficient ($cm^2\ s^{-1}$)
D_{m}	salt diffusion coefficient of a model nanostructured electrolyte ($cm^2\ s^{-1}$)
D_{n}	normalized salt diffusion coefficient
DIS	disordered morphology
f	morphology factor
F	faraday's constant (96,485 C mol^{-1})
GYR	double gyroid morphology with a minority PEO phase

GYR'	double gyroid morphology with a minority PS phase
HEX	hexagonally packed cylinders morphology with PEO-rich cylinders
HEX'	hexagonally packed cylinders morphology with PS-rich cylinders
i_{Ω}	initial current density calculated using Ohm's law (mA cm^{-2})
i_{ss}	current density measured at steady-state during dc polarization (mA cm^{-2})
L	electrolyte thickness (cm)
LAM	lamellar morphology with alternating PS- and PEO-rich domains
LiTFSI	bis(trifluoromethane)sulfonimide lithium salt
m	molality of the conducting domain (mol kg^{-1})
m_{r}	molality of the conducting domain of the reference electrolyte in a concentration cell (mol kg^{-1})
M_{EO}	molar mass of an ethylene oxide monomer (44.05 g mol^{-1})
M_{LiTFSI}	molar mass of LiTFSI (287.08 g mol^{-1})
M_{PEO}	number averaged molecular weight of PEO (kg mol^{-1})
M_{PS}	number averaged molecular weight of PS (kg mol^{-1})
M_{S}	molar mass of a styrene monomer (104.1 g mol^{-1})
N	number of repeat units in a polymer or block copolymer chain
N_A	Avogadro's number (6.022×10^{23} mol^{-1})
N_{i}	number of repeat units of component *i* in a block copolymer chain
PEO	poly(ethylene oxide)
PS	polystyrene
r	molar ratio of lithium ions to ethylene oxide moieties, $r = [Li]/[EO]$
R	ideal gas constant (8.314 J mol^{-1} K^{-1})
R_{b}	bulk resistance of the electrolyte measured by ac impedance spectroscopy (Ω)
$R_{i,0}$	interfacial resistance measured by ac impedance spectroscopy before dc polarization (Ω)
$R_{i,ss}$	interfacial resistance measured by ac impedance spectroscopy at steady-state during dc polarization (Ω)
SAXS	small angle X-ray scattering
SEO	polystyrene-*block*-polyethylene
SEO(*x*-*y*)	SEO with M_{PS} = *x* kg mol^{-1} and M_{PEO} = *y* kg mol^{-1}
t	time (s)
t_{+}^{0}	transference number of the cation with respect to the velocity of the solvent
T	temperature (K)
T_{f}	thermodynamic factor
U	open circuit potential of a concentration cell (mV)
U'	open circuit potential of a concentration cell offset by a constant, C (mV)
ΔV	dc potential drop applied across a symmetric cell (mV)
v_{c}	volume of the conducting phase per ethylene oxide monomer (nm^3)
v_{EO}	volume of the ethylene oxide monomer at 90 °C (0.0682 nm^3)
v_{S}	volume of the styrene monomer at 90 °C (0.167 nm^3)

z_+	charge number of the cation

GREEK

γ_{+-}	mean molal activity coefficient of the electrolyte
κ	ionic conductivity of an electrolyte (S cm^{-1})
κ_{m}	ionic conductivity of a model nanostructured electrolyte (S cm^{-1})
κ_{n}	normalized ionic conductivity
κ_{nb}	ionic conductivity of an electrolyte measured in a cell with non-blocking electrodes (S cm^{-1})
μ_+, μ_-	electrochemical potential of the cation and anion, respectively (J mol^{-1})
μ_{e}	electrochemical potential of the electrolyte (J mol^{-1})
ν_+, ν_-	number of cation and anions, respectively, in the dissociated salt
ρ_+	current fraction
ρ_{c}	density of the conducting phase (g cm^{-3})
ρ_{PEO}	density of PEO at 90 °C (1.07 g cm^{-3})
ρ_{PS}	density of PS at 90 °C (1.03 g cm^{-3})
τ	tortuosity factor
ϕ_{c}	volume fraction of the conducting phase in a salty block copolymer
ϕ_{EO}	volume fraction of PEO in a neat block copolymer

AUTHOR INFORMATION

Corresponding Author

*E-mail: nbalsara@berkeley.edu

Notes

The authors declare no competing financial interest.

ACKNOWLEDGMENT

This work was supported by the Assistant Secretary for Energy Efficiency and Renewable Energy, Office of Vehicle Technologies of the U.S. Department of Energy under Contract DE-AC02-05CH11231 under the Battery Materials Research Program.

REFERENCES

(1) Galizia, M.; Chi, W. S.; Smith, Z. P.; Merkel, T. C.; Baker, R. W.; Freeman, B. D. *50th Anniversary Perspective* : Polymers and Mixed Matrix Membranes for Gas and Vapor Separation: A Review and Prospective Opportunities. *Macromolecules* **2017**, *50* (20), 7809–7843.

(2) Robeson, L. M. Polymer Membranes for Gas Separation. *Curr. Opin. Solid State Mater. Sci.* **1999**, *4* (6), 549–552.

(3) Werber, J. R.; Osuji, C. O.; Elimelech, M. Materials for Next-Generation Desalination and Water Purification Membranes. *Nature Reviews Materials* **2016**, *1*, 16018.

(4) Ma, H.; Burger, C.; Hsiao, B. S.; Chu, B. Highly Permeable Polymer Membranes Containing Directed Channels for Water Purification. *ACS Macro Lett.* **2012**, *1* (6), 723–726.

(5) Prater, K. The Renaissance of the Solid Polymer Fuel Cell. *J. Power Sources* **1990**, *29* (1–2), 239–250.

(6) Wang, Y.; Ruiz Diaz, D. F.; Chen, K. S.; Wang, Z.; Adroher, X. C. Materials, Technological Status, and Fundamentals of PEM Fuel Cells – A Review. *Mater. Today* **2019**. In Press. DOI: j.mattod.2019.06.005.

(7) DeLuca, N. W.; Elabd, Y. A. Polymer Electrolyte Membranes for the Direct Methanol Fuel Cell: A Review. *J. Polym. Sci. Part B Polym. Phys.* **2006**, *44* (16), 2201–2225.

(8) Fenton, D. E.; Parker, M.; Wright, P. V. Complexes of Alkali Metal Ions with Poly(Ethylene Oxide). *Polymer* **1973**, 14, 589.

(9) Berthier, C.; Gorecki, W.; Minier, M.; Armand, M. B.; Chabagno, J. M.; Rigaud, P.

Microscopic Investigation of Ionic Conductivity in Alkali Metal Salts-Poly(ethylene oxide) Adducts, *Solid State Ion.* **1983**, *11*, 91-95.

(10) Hallinan, D. T.; Mullin, S. A.; Stone, G. M.; Balsara, N. P. Lithium Metal Stability in Batteries with Block Copolymer Electrolytes. *J. Electrochem. Soc.* **2013**, *160* (3), A464–A470.

(11) Singh, M.; Odusanya, O.; Wilmes, G. M.; Eitouni, H. B.; Gomez, E. D.; Patel, A. J.; Chen, V. L.; Park, M. J.; Fragouli, P.; Iatrou, H.; et al. Effect of Molecular Weight on the Mechanical and Electrical Properties of Block Copolymer Electrolytes. *Macromolecules* **2007**, *40* (13), 4578-4585.

(12) Long, L.; Wang, S.; Xiao, M.; Meng, Y. Polymer Electrolytes for Lithium Polymer Batteries. *J. Mater. Chem. A*, **2016**, *4*, 10038.

(13) Soo, P. P.; Huang, B.; Jang, Y. I. I.; Chiang, Y. M.; Sadoway, D. R.; Mayes, A. M. Rubbery Block Copolymer Electrolytes for Solid-State Rechargeable Lithium Batteries. *J. Electrochem. Soc.* **1999**, *146* (1), 32–37.

(14) Arbizzani, C.; Mastragostino, M.; Hamaide, T.; Guyot, A. An All Solid-State Polymer-Polymer Electrolyte-Lithium Rechargeable Battery for Room Temperature Applications. *Electrochim. Acta* **1990**, *35* (11–12), 1781–1785.

(15) Rzayev, J.; Hillmyer, M. A. Nanoporous Polystyrene Containing Hydrophilic Pores from an ABC Triblock Copolymer Precursor. *Macromolecules* **2005**, *38* (1), 3-5**.**

(16) Young, W.-S.; Kuan, W.-F.; Epps, T. H. Block Copolymer Electrolytes for Rechargeable Lithium Batteries. *J. Polym. Sci. Part B Polym. Phys.* **2014**, *52* (1), 1–16.

(17) Barteau, K. P.; Wolffs, M.; Lynd, N. A.; Fredrickson, G. H.; Kramer, E. J.; Hawker, C. J. Allyl Glycidyl Ether-Based Polymer Electrolytes for Room Temperature Lithium Batteries.

Macromolecules **2013**, *46* (22), 8988–8994.

(18) Villaluenga, I.; Chen, X. C.; Devaux, D.; Hallinan, D. T.; Balsara, N. P. Nanoparticle-Driven Assembly of Highly Conducting Hybrid Block Copolymer Electrolytes. *Macromolecules* **2015**, *48* (2), 358–364.

(19) Balsara, N. P.; Singh, M.; Eitouni, H. B.; Comex, E. D. "High Elastic Modulus Polymer Electrolytes," filed by the Regents of the University of California on April 3, 2007. Publication date: Oct 22, 2013. US Patent Application 12/225, 934. PCT Number: PCT/US2007/008435.

(20) Cheng, X.-B.; Zhang, R.; Zhao, C.-Z.; Zhang, Q. Toward Safe Lithium Metal Anode in Rechargeable Batteries: A Review. *Chem. Rev.* **2017**, *117* (15), 10403–10473.

(21) Frenck, L.; Sethi, G. K.; Maslyn, J. A.; Balsara, N. P. Factors That Control the Formation of Dendrites and Other Morphologies on Lithium Metal Anodes. *Front. Energy Res.* **2019**, *7*, 115.

(22) Maslyn, J. A.; Loo, W. S.; McEntush, K. D.; Oh, H. J.; Harry, K. J.; Parkinson, D. Y.; Balsara, N. P. Growth of Lithium Dendrites and Globules through a Solid Block Copolymer Electrolyte as a Function of Current Density. *J. Phys. Chem. C* **2018**, *122* (47), 26797–26804.

(23) Sax, J.; Ottino, J. M. Modeling of Transport of Small Molecules in Polymer Blends: Application of Effective Medium Theory. *Polym. Eng. Sci.* **1983**, *23* (1 l), 165–176.

(24) Irwin, M. T.; Hickey, R. J.; Xie, S.; So, S.; Bates, F. S.; Lodge, T. P. Structure-Conductivity Relationships in Ordered and Disordered Salt-Doped Diblock Copolymer/Homopolymer Blends. *Macromolecules* **2016**, *49* (18), 6928–6939.

(25) Cho, B. K.; Jain, A.; Gruner, S. M.; Wiesner, U. Mesophase Structure-Mechanical and Ionic

Transport Correlations in Extended Amphiphilic Dendrons. *Science* **2004**, *305* (5690), 1598–1601.

(26) Majewski, P. W.; Gopinadhan, M.; Jang, W.-S.; Lutkenhaus, J. L.; Osuji, C. O. Anisotropic Ionic Conductivity in Block Copolymer Membranes by Magnetic Field Alignment. *J. Am. Chem. Soc.* **2010**, *132* (49), 17516–17522.

(27) Bates, F. S.; Fredrickson, G. H. Block Copolymer Thermodynamics: Theory and Experiment. *Annu. Rev. Phys. Chem.* **1990**, *41* (1), 525–557.

(28) Teran, A. A.; Balsara, N. P. Thermodynamics of Block Copolymers with and without Salt. *J. Phys. Chem. B* **2014**, *118* (1), 4–17.

(29) Loo, W. S.; Galluzzo, M. D.; Li, X.; Maslyn, J. A.; Oh, H. J.; Mongcopa, K. I.; Zhu, C.; Wang, A. A.; Wang, X.; Garetz, B. A.; et al. Phase Behavior of Mixtures of Block Copolymers and a Lithium Salt. *J. Phys. Chem. B* **2018**, *122* (33), 8065–8074.

(30) Shen, K.-H.; Brown, J. R.; Hall, L. M. Diffusion in Lamellae, Cylinders, and Double Gyroid Block Copolymer Nanostructures. *ACS Macro Lett.* **2018**, 1092–1098.

(31) Newman, J.; Thomas-Alyea, K. E. *Electrochemical Systems*; 2004.

(32) Pesko, D. M.; Feng, Z.; Sawhney, S.; Newman, J.; Srinivasan, V.; Balsara, N. P. Comparing Cycling Characteristics of Symmetric Lithium-Polymer-Lithium Cells with Theoretical Predictions. *J. Electrochem. Soc.* **2018**, *165* (13), A3186–A3194.

(33) Balsara, N. P.; Newman, J. Relationship between Steady-State Current in Symmetric Cells and Transference Number of Electrolytes Comprising Univalent and Multivalent Ions. *J. Electrochem. Soc.* **2015**, *162* (14), A2720–A2722.

(34) Gribble, D. A.; Frenck, L.; Shah, D. B.; Maslyn, J. A.; Loo, W. S.; Mongcopa, K. I. S.; Pesko, D. M.; Balsara, N. P. Comparing Experimental Measurements of Limiting Current

in Polymer Electrolytes with Theoretical Predictions. *J. Electrochem. Soc.* **2019**, *166* (14), A3228–A3234.

(35) Hadjichristidis, N.; Iatrou, H.; Pispas, S.; Pitsikalis, M. Anionic Polymerization: High Vacuum Techniques. *J. Polym. Sci. Part A Polym. Chem.* **2000**, *38* (18), 3211–3234.

(36) Mark, J. E., *Physical Properties of Polymers Handbook*, 2nd ed.; Springer: Philadelphia, PA, 2007.

(37) Yuan, R.; Teran, A. A.; Gurevitch, I.; Mullin, S. A.; Wanakule, N. S.; Balsara, N. P. Ionic Conductivity of Low Molecular Weight Block Copolymer Electrolytes. Macromolecules **2013**, *46*, 914-921.

(38) Villaluenga, I.; Pesko, D. M.; Timachova, K.; Feng, Z.; Newman, J.; Srinivasan, V.; Balsara, N. P. Negative Stefan-Maxwell Diffusion Coefficients and Complete Electrochemical Transport Characterization of Homopolymer and Block Copolymer Electrolytes. *J. Electrochem. Soc.* **2018**, *165* (11), A2766–A2773.

(39) Gomez, E. D.; Panday, A.; Feng, E. H.; Chen, V.; Stone, G. M.; Minor, A. M.; Kisielowski, C.; Downing, K. H.; Borodin, O.; Smith, G. D.; Balsara, N.P. Effect of Ion Distribution on Conductivity of Block Copolymer Electrolytes. *Nano Lett.* **2009**, *9* (3), 1212–1216.

(40) Gilbert, J. B.; Luo, M.; Shelton, C. K.; Rubner, M. F.; Cohen, R. E.; Epps, T. H. Determination of Lithium-Ion Distributions in Nanostructured Block Polymer Electrolyte Thin Films by X-Ray Photoelectron Spectroscopy Depth Profiling. *ACS Nano* **2015**, *9* (1), 512–520.

(41) Gartner, T. E.; Morris, M. A.; Shelton, C. K.; Dura, J. A.; Epps, T. H. Quantifying Lithium Salt and Polymer Density Distributions in Nanostructured Ion-Conducting Block Polymers. *Macromolecules* **2018**, *51* (5), 1917–1926.

(42) Pesko, D. M.; Timachova, K.; Bhattacharya, R.; Smith, M. C.; Villaluenga, I.; Newman, J.; Balsara, N. P. Negative Transference Numbers in Poly(Ethylene Oxide)-Based Electrolytes. *J. Electrochem. Soc.* **2017**, *164* (11), E3569–E3575.

(43) Fredrickson, G. H.; Helfand, E. Fluctuation Effects in the Theory of Microphase Separation in Block Copolymers. *J. Chem. Phys.* **1987**, *87* (1), 697–705.

(44) Qin, J.; de Pablo, J. J. Ordering Transition in Salt-Doped Diblock Copolymers. *Macromolecules* **2016**, *49* (9), 3630–3638.

(45) Nakamura, I.; Wang, Z.-G. Salt-Doped Block Copolymers: Ion Distribution, Domain Spacing and Effective χ Parameter. *Soft Matter* **2012**, *8* (36), 9356.

(46) Loo, W. S.; Sethi, G. K.; Teran, A. A.; Galluzzo, M. D.; Maslyn, J. A.; Oh, H. J.; Mongcopa, K. I.; Balsara, N. P. Composition Dependence of the Flory–Huggins Interaction Parameters of Block Copolymer Electrolytes and the Isotaksis Point. *Macromolecules* **2019**, *52* (15), 5590–5601.

(47) Panday, A.; Mullin, S.; Gomez, E. D.; Wanakule, N.; Chen, V. L.; Hexemer, A.; Pople, J.; Balsara, N. P. Effect of Molecular Weight and Salt Concentration on Conductivity of Block Copolymer Electrolytes. *Macromolecules* **2009**.

(48) Chintapalli, M.; Le, T. N. P.; Venkatesan, N. R.; Mackay, N. G.; Rojas, A. A.; Thelen, J. L.; Chen, X. C.; Devaux, D.; Balsara, N. P. Structure and Ionic Conductivity of Polystyrene-*Block* -Poly(Ethylene Oxide) Electrolytes in the High Salt Concentration Limit. *Macromolecules* **2016**, *49* (5), 1770–1780.

(49) Timachova, K.; Villaluenge, I.; Cirrincione, L.; Gobet, M.; Bhattacharya, R.; Jiang, X.; Newman, J.; Madsen, L. A.; Greenbaum Steven G.; Balsara, N. P. Anisotropic Ion Diffusion and Electrochemically Driven Transport in Nanostructured Block Copolymer Electrolytes.

J. Phys. Chem. B **2018**, *122* (4).

(50) Mullin, S. A.; Teran, A. A.; Yuan, R.; Balsara, N. P. Effect of Thermal History on the Ionic Conductivity of Block Copolymer Electrolytes. *J. Polym. Sci. Part B Polym. Phys.* **2013**, *51* (12), 927–934.

(51) Galluzzo, M. D.; Maslyn, J. A.; Shah, D. B.; Balsara, N. P. Ohm's Law for Ion Conduction in Lithium and beyond-Lithium Battery Electrolytes. *J. Chem. Phys.* **2019**, *151* (2), 020901.

(52) Bruce, P. G.; Vincent, C. A. Steady State Current Flow in Solid Binary Electrolyte Cells. *J. Electroanal. Chem. Interfacial Electrochem.* **1987**, *225* (1–2), 1–17.

(53) Evans, J.; Vincent, C. A.; Bruce, P. G. Electrochemical Measurement of Transference Numbers in Polymer Electrolytes. *Polymer* **1987**, *28* (13), 2324–2328.

(54) Bruce, P.G.; Gray, F.M. in *Solid State Electrochemistry*, edited by P. G. Bruce (Cambridge University Press, **1995**), pp. 157–158.

(55) Arges, C. G.; Kambe, Y.; Suh, H. S.; Ocola, L. E.; Nealey, P. F. Perpendicularly Aligned, Anion Conducting Nanochannels in Block Copolymer Electrolyte Films. *Chem. Mater.* **2016**, *28* (5), 1377–1389.

(56) Arges, C. G.; Kambe, Y.; Dolejsi, M.; Wu, G.-P.; Segal-Pertz, T.; Ren, J.; Cao, C.; Craig, G. S. W.; Nealey, P. F. Interconnected Ionic Domains Enhance Conductivity in Microphase Separated Block Copolymer Electrolytes. *J. Mater. Chem. A* **2017**, *5* (11), 5619–5629.

(57) Sharon, D.; Bennington, P.; Liu, C.; Kambe, Y.; Dong, B. X.; Burnett, V. F.; Dolejsi, M.; Grocke, G.; Patel, S. N.; Nealey, P. F. Interrogation of Electrochemical Properties of Polymer Electrolyte Thin Films with Interdigitated Electrodes. *J. Electrochem. Soc.* **2018**, *165* (16), H1028–H1039.

(58) Kim, S. H.; Misner, M. J.; Yang, L.; Gang, O.; Ocko, B. M.; Russell, T. P. Salt

Complexation in Block Copolymer Thin Films. *Macromolecules* **2006**, *39* (24), 8473–8479.

(59) Balsara, N. P.; Garetz, B. A.; Dai, H. J. Relationship between Birefringence and the Structure of Ordered Block Copolymer Materials. *Macromolecules* **1992**, *25* (22), 6072–6074.

(60) Mongcopa, K. I. S.; Tyagi, M.; Mailoa, J. P.; Samsonidze, G.; Kozinsky, B.; Mullin, S. A.; Gribble, D. A.; Watanabe, H.; Balsara, N. P. Relationship between Segmental Dynamics Measured by Quasi-Elastic Neutron Scattering and Conductivity in Polymer Electrolytes. *ACS Macro Lett.* **2018**, *7* (4), 504–508.

(61) Chintapalli, M.; Chen, X. C.; Thelen, J. L.; Teran, A. A.; Wang, X.; Garetz, B. A.; Balsara, N. P. Effect of Grain Size on the Ionic Conductivity of a Block Copolymer Electrolyte. *Macromolecules* **2014**, *47* (15), 5424–5431.

(62) Ma, Y.; Doyle, M.; Fuller, T. F.; Doeff, M. M.; Jonghe, L. C. De; Newman, J. The Measurement of a Complete Set of Transport Properties for a Concentrated Solid Polymer Electrolyte Solution. *J. Electrochem. Soc.* **1995**, *142* (6), 1859.

(63) Hallinan, D. T.; Villaluenga, I.; Balsara, N. P. Polymer and Composite Electrolytes. *MRS Bull.* **2018**, *43* (10), 759–767.

(64) Hallinan, D. T.; Balsara, N. P. Polymer Electrolytes. *Annu. Rev. Mater. Res.* **2013**, *43* (1), 503–525.

(65) Desmet, G.; Deridder, S. Effective Medium Theory Expressions for the Effective Diffusion in Chromatographic Beds Filled with Porous, Non-Porous and Porous-Shell Particles and Cylinders. Part I: Theory. *J. Chromatogr. A* **2011**, *1218* (1), 32–45.

(66) Teran, A. A.; Tang, M. H.; Mullin, S. A.; Balsara, N. P. Effect of Molecular Weight on Conductivity of Polymer Electrolytes. *Solid State Ionics* **2011**, *203* (1), 18–21.

(67) Shi, J.; Vincent, C. A. The Effect of Molecular Weight on Cation Mobility in Polymer Electrolytes. *Solid State Ionics* **1993**, *60* (1–3), 11–17.

(68) Molinari, N.; Mailoa, J. P.; Kozinsky, B. Effect of Salt Concentration on Ion Clustering and Transport in Polymer Solid Electrolytes: A Molecular Dynamics Study of PEO–LiTFSI. *Chem. Mater.* **2018**, *30* (18), 6298–6306.

(69) Seo, Y.; Shen, K.-H.; Brown, J. R.; Hall, L. M. Role of Solvation on Diffusion of Ions in Diblock Copolymers: Understanding the Molecular Weight Effect through Modeling. *J. Am. Chem. Soc.* **2019**, jacs.9b07227.

(70) Watanabe, M.; Nagano, S.; Sanui, K.; Ogata, N. Estimation of Li+ Transport Number in Polymer Electrolytes by the Combination of Complex Impedance and Potentiostatic Polarization Measurements. *Solid State Ionics* **1988**, *28–30*, 911–917.

(71) Hiller, M. M.; Joost, M.; Gores, H. J.; Passerini, S.; Wiemhöfer, H.-D. The Influence of Interface Polarization on the Determination of Lithium Transference Numbers of Salt in Polyethylene Oxide Electrolytes. *Electrochim. Acta* **2013**, *114*, 21–29.

(72) Shah, D. B.; Nguyen, H. Q.; Grundy, L. S.; Olson, K. R.; Mecham, S. J.; DeSimone, J. M.; Balsara, N. P. Difference between Approximate and Rigorously Measured Transference Numbers in Fluorinated Electrolytes. *Phys. Chem. Chem. Phys.* **2019**, *21* (15), 7857–7866.

(73) Balsara, N. P.; Newman, J. Relationship between Steady-State Current in Symmetric Cells and Transference Number of Electrolytes Comprising Univalent and Multivalent Ions. *J. Electrochem. Soc.* **2015**, *162* (14), A2720–A2722.

(74) Chintapalli, M.; Timachova, K.; Olson, K. R.; Mecham, S. J.; Devaux, D.; Desimone, J. M.; Balsara, N. P. Relationship between Conductivity, Ion Diffusion, and Transference Number in Perfluoropolyether Electrolytes. *Macromolecules* **2016**, *49* (9), 3508-3515.

(75) Piszcz, M.; Garcia-Calvo, O.; Oteo, U.; Lopez del Amo, J. M.; Li, C.; Rodriguez-Martinez, L. M.; Youcef, H. Ben; Lago, N.; Thielen, J.; Armand, M. New Single Ion Conducting Blend Based on PEO and PA-LiTFSI. *Electrochim. Acta* **2017**, *255*, 48–54.

(76) Porcarelli, L.; Gerbaldi, C.; Bella, F.; Nair, J. R. Super Soft All-Ethylene Oxide Polymer Electrolyte for Safe All-Solid Lithium Batteries. *Sci. Rep.* **2016**, *6* (1), 19892.

(77) Craig, N.; Mullin, S. A.; Pratt, R.; Crane, G. B. Determination of Transference Number and Thermodynamic Factor by Use of Anion-Exchange Concentration Cells and Concentration Cells. *J. Electrochem. Soc.* **2019**, *166* (13), A2769–A2775.

(78) Morris, M. A.; Gartner, T. E.; Epps, T. H. Tuning Block Polymer Structure, Properties, and Processability for the Design of Efficient Nanostructured Materials Systems. *Macromol. Chem. Phys.* **2017**, *218* (5), 1600513.

(79) Jo, G.; Ahn, H.; Park, M. J. Simple Route for Tuning the Morphology and Conductivity of Polymer Electrolytes: One End Functional Group Is Enough. *ACS Macro Lett.* **2013**, *2* (11), 990–995.

(80) Wanakule, N. S.; Panday, A.; Mullin, S. A.; Gann, E.; Hexemer, A.; Balsara, N. P. Ionic Conductivity of Block Copolymer Electrolytes in the Vicinity of Order-Disorder and Order-Order Transitions. *Macromolecules* **2009**, *42* (15), 5642–5651.

(81) Jung, H. Y.; Mandal, P.; Jo, G.; Kim, O.; Kim, M.; Kwak, K.; Park, M. J. Modulating Ion Transport and Self-Assembly of Polymer Electrolytes via End-Group Chemistry. *Macromolecules* **2017**, *50* (8), 3224–3233.

(82) Majewski, P. W.; Gopinadhan, M.; Osuji, C. O. The Effects of Magnetic Field Alignment on Lithium Ion Transport in a Polymer Electrolyte Membrane with Lamellar Morphology. *Polymers (Basel).* **2019**, *11* (5), 887.

TOC GRAPHICS